UnderOak Observer

Issue 2 · October-December 2011

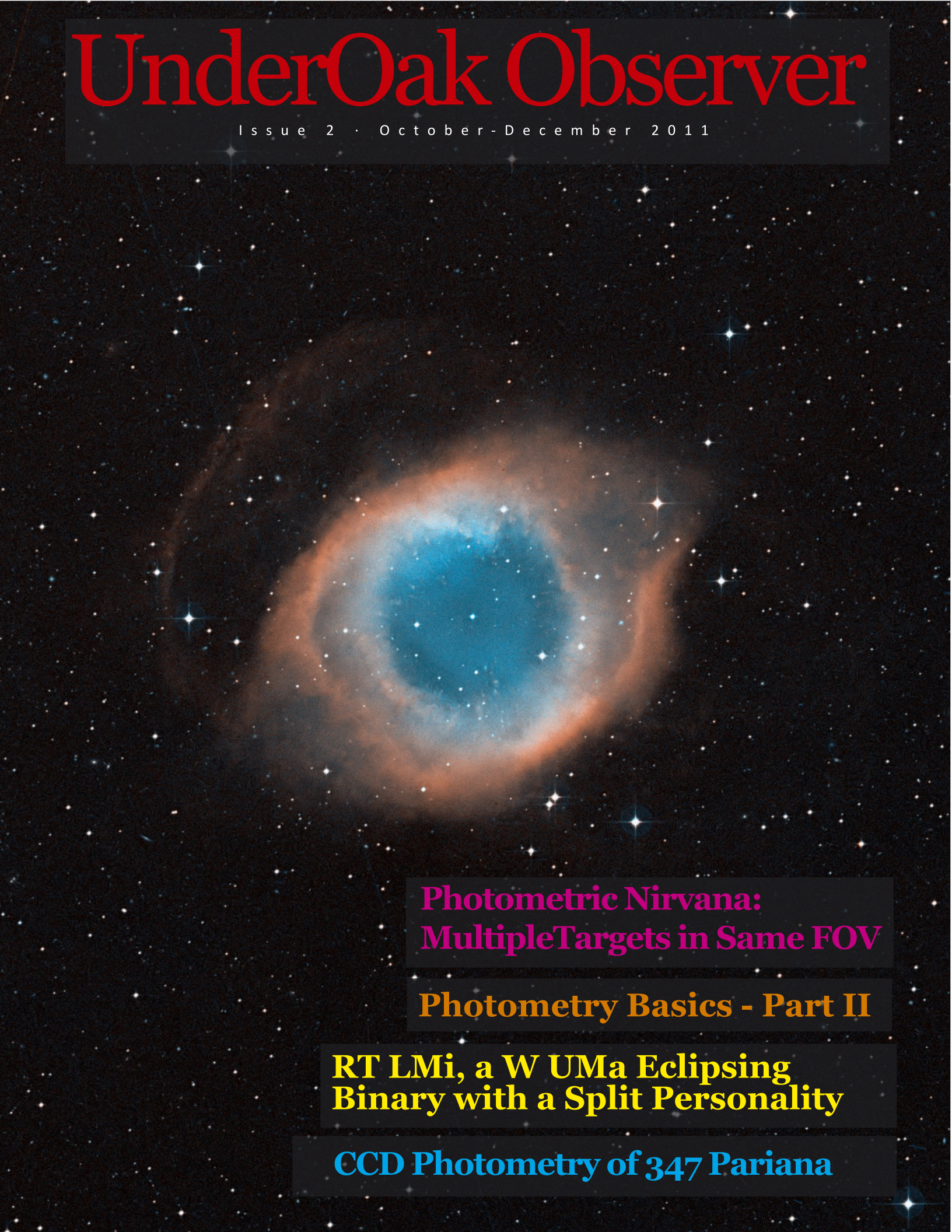

Photometric Nirvana: MultipleTargets in Same FOV

Photometry Basics - Part II

RT LMi, a W UMa Eclipsing Binary with a Split Personality

CCD Photometry of 347 Pariana

CCD Photometry of the Minor Planet 347 Pariana

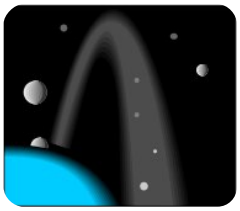

Abstract

CCD images of 347 Pariana were acquired on three nights between 11May2008 and 02June2008 and then used to determine the synodic period (4.05299 hr) for this main belt asteroid.

Introduction

347 Pariana (~51.4 km) is a main belt asteroid discovered (1892) by the French astronomer Auguste Charlois. Over a 17 year period between 1887 and 1904, Charlois discovered 99 minor planets while observing in Nice. As a tragic side note, before Charlois was able to make his 100th asteroid discovery, he was murdered at age 46 by the brother of his first wife. M-type minor planets like 347 Pariana are highly reflective (albedo=0.1-0.2) and considered to be a potential source of iron meteorites. The first photometric light curves were generated by Lagerkvist et al in 1992. Over the next 20 years only four other complete light curves from this asteroid were reported in the literature including those produced by Denchev (2000), Majcen and Wetterer (1999) and Caspari (2010). Bolstered by two new light curves in 2009, Caspari (2010) was also able to propose a preliminary three dimensional structure using inverse shape modeling (Kaasalainen et al 2001).

Results and Discussion

For this study a focal reduced (f/6.3) 0.2-m Schmidt-Cassegrain telescope was coupled with a Peltier cooled (-10°C) SBIG ST-402ME CCD camera mounted at prime focus. To ensure accurate timings, the computer clock was updated via the Internet Time Server before every run. I_c (May 11 and May 29) and clear filter (June 2) images were taken with 60 sec exposures continually captured during each session. Raw lights, darks and flats acquired using CCDSoft 5 were calibrated and registered with AIP4WIN (Berry and Burnell 2008). MPO Canopus (Warner 2010) was used to generate light curves by differential aperture photometry by including four non-varying comparison stars captured each evening in the same FOV. A total of 457 light curve values were acquired over 22 days; data were not reduced to standard magnitudes but were light time corrected.

MPO Canopus yielded a period solution (Fig. 1) for the folded data sets using Fourier analysis (Harris 1989). The synodic period (4.0529999 ± 0.0000001 hr) was in good agreement with rotational periods for this asteroid published by others and that reported by the "Small-Body Database Browser" at the JPL Solar System Dynamics website. In addition, the light curve amplitude (~0.2 mag) was within the range (0.175-0.5 mag) observed in previous investigations. Relevant aspect parameters (phase angle, phase angle bisector ecliptic longtitude (L_{PAB}) and phase angle bisector ecliptic latitude (B_{PAB})) for 347 Pariana taken at the mid-point from each session are tabulated below. Phase angle is the Sun-asteroid-observer angle while L_{PAB} and B_{PAB} are the ecliptic coordinates of the phase angle bisector which define the pole orientation of an asteroid at a particular time.

Acknowledgement

The SAO/NASA Astrophysics Data_System (http://adsabs.harvard.edu/abstract_service.html) was used to conduct literature searches in support of this study.

References

Berry, R. and Burnell, J. 2008, AIP4WIN version 2.3.1, Willmann-Bell, Inc, Richmond, VA.

Caspari, P. 2010, The Minor Planet Bulletin, 37, 107.

Denchev, P. 2000, Planetary and Space Science, 48, 987.

Harris, A.W., Young, J.W., Bowell, E., Martin, L. J., Millis, R. L., Poutanen, M., Scaltriti, F., Zappala, V., Schober, H. J., Debehogne, H, and Zeigler, K. 1989, Icarus 77, 171.

JPL Solar System Dynamics website (http://ssd.jpl.nasa.gov/sbdb.cgi)

Kaasalainen, M., Torppa, J. and Piironen, J. 2001, Bulletin of the American Astronomical Society, 33, 1153.

Lagerkvist, C.-I., Magnusson, P., Debehogne, H.,

Hoffmann, M., Erikson, A., de Campos, A. and Cutispoto, G. 1992, Astronomy and Astrophysics Supplement Series, 3, 461.
Majcen, S. and Wetterer, C.J. 1999, The Minor Planet Bulletin, 26, 29.
Warner, B.D. 2010, MPO Canopus version 10.3.0.2. Bdw Publishing, Colorado Springs, CO.

UT Date (2008)	No. Obs	Phase Angle	L_{PAB}	B_{PAB}	%Phase Coverage
May 11	209	16.3	202.7	13.0	74.4
May 29	96	21.2	205.3	11.4	39.9
June 2	152	22.1	206.1	11.1	88.3

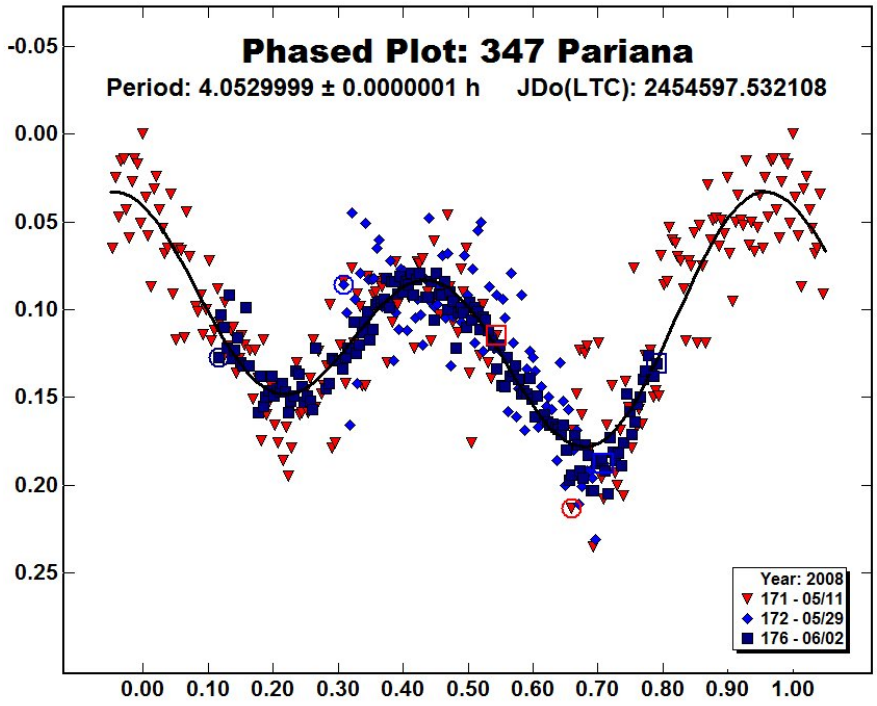

Figure 1
Folded light curves (phase vs relative flux) from the 2008 photometric campaign of 347 Pariana

Caveats:

The "UnderOak Observer" is published advertisement free using Scribus (v1.3.3.14). Its intent is both entertainment and informational. Every reasonable effort is made to verify facts and avoid personal bias, however, the reader bears full responsibility for actually listening to what I have to say.

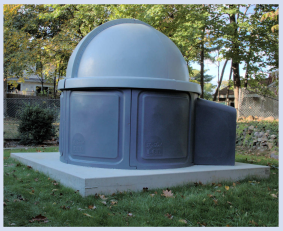

Cover Page Art:

Helix Nebula (NGC 7293) in Aquarius. Color was rendered using Registar after synthesizing green from red and blue images downloaded with the DSS Plate Finder (http://archive.stsci.edu/cgi-bin/dss_plate_finder).

Editor: Kevin B. Alton
Writer: Kevin B. Alton

Public Access:

Free access to any light curve data associated with research published in the UO can be obtained by request (mail@underoakobservatory.com)

Photometry Basics

Part II: Modeling and Graphical Software

This issue I'll provide a brief overview of software available for 1) producing and analyzing O-C diagrams 2) determining the periodicity of light curves from variable stars or minor planets and 3) fitting light curve data from eclipsing binaries using Roche modeling derived from the Wilson-Devinney code. The good news is that many of these data analysis tools exist as fully functional public domain applications written for PC-, Mac- or Linux-based computers. With the exception of Excel, all of the corresponding commercial packages are priced at or under $100 US.

Preparation and Analysis of O-C Diagrams

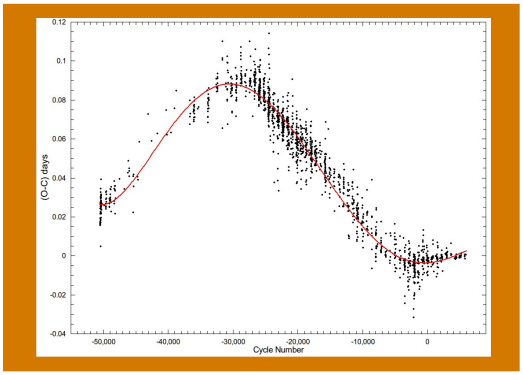

Similar to the temporal relationship between climate and weather, O-C diagrams are helpful for looking at long-term changes in a variable star or system rather than the day-to-day changes that might be observed with individual light curves. The underlying data are derived from accurately observed timings at light curve minima (or maxima) and any difference that might occur when compared to predicted values based upon light curve periodicity obtained from previous epochs. The mathematics involved is not particularly challenging, but very tedious and best handled with a spreadsheet like Excel (http://office.microsoft.com/en-us/excel/) or its public domain doppelgängers OpenOffice (http://www.openoffice.org/) and LibreOffice (http://www.libreoffice.org/). Depending on skill level, all of these spreadsheet applications are capable of fitting curves by linear and non-linear regression methods and producing publication quality graphics. Thousands of Excel O-C spreadsheets from eclipsing binaries are available at the AASVO website (http://www.aavso.org/bob-nelsons-o-c-files) so that in many cases you will not have to start from scratch. Each of these readily import into OpenOffice or LibreOffice Calc. Alternatively, as was mentioned in Issue 1 (2011) of this e-magazine, QtiPlot (http://soft.proindependent.com/qtiplot.html) offers a sophisticated interface for curve fitting and is capable of rendering very high quality charts and figures. Finally, there are many different methods to estimate the observed time(s)-of-minima from your own light curve data which are needed to produce an O-C diagram. Most of these including parabolic fit, tracing paper, bisecting chords, Kwee and van Woerden (1956), Fourier fit, and sliding integrations (Ghedini 1981) have been conveniently bundled together in a single application appropriately named "Minima" which can be downloaded from Bob Nelson's astronomy software website (http://members.shaw.ca/bob.nelson/software1.htm).

Light Curve Period Study

One of the primary goals in measuring the time-dependent luminous intensity from a putative variable object is to determine whether there is predictable periodicity associated with detectable changes in magnitude. Photometric data are typically gathered during different observing sessions which means they need to be folded together to produce a composite light curve. Fortunately this task is made possible by mathematically sophisticated programs designed to determine whether there is any statistically meaningful periodicity (or multiple periodicities) associated with the rise and fall of light intensity. The Fourier transform routine (Harris et al 1989) built into MPO/Canopus (http://www.minorplanetobserver.com /MPOSoftware/MPOCanopus.htm) is usually adequate for characterizing the primary period associated with light curves from eclipsing binary stars and minor planets. I often use Peranso (http://www.peranso.com/) which has a comprehensive repertoire of Fourier and statistical methods to independently confirm a period determination. In some cases there may be more than one period associated with variations in a light curve. This is particularly true for variable star types (eg δ Scuti, RR Lyrae and Cepheids) which pulsate or oscillate in a regular fashion. The amplitude of a primary period

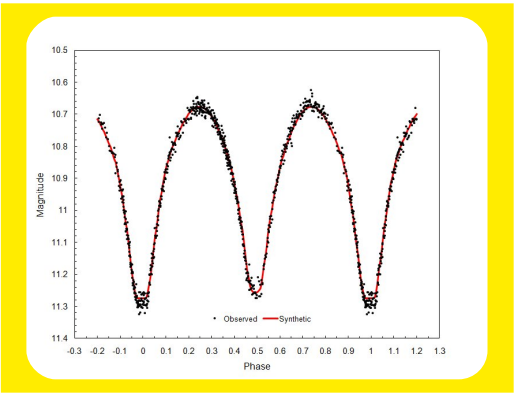

can completely overwhelm underlying periods associated with milli-magnitude changes and may need to be subtracted out using a process called pre-whitening. The residual signal can be sequentially tested for periodicity until all that remains is noise. Peranso has a routine for pre-whitening which provides immediate graphical feedback. Period04 (Lenz and Breger 2005) another Windows, Mac OS X 10.6, and Linux compatible tool residing in the public domain (http://www.univie.ac.at/tops/Period04/), features a discrete Fourier transform algorithm which can very efficiently tease out and test the statistical significance of any underlying periodicity (fundamental, harmonic or overtones). The last public domain software package to consider is entitled FAMIAS, an acronym for "Frequency Analysis and Mode Identification for Asteroseismology" (Zima 2008). FAMIAS is programmed in C++, compiled for use on Ubuntu Linux and Mac OS X 10.5 platforms and one click away from download at http://www.ster.kuleuven.be/~zima/famias/. I have a working version running under Ubuntu 10.10 but have not had a chance to put it through its paces using light curve data from a few pulsating variables that were recently studied at UO. FAMIAS is not only designed to detect multiple periodicities using Fourier transform or non-linear least squares fitting but also to identify pulsation modes.

Roche Modeling of Eclipsing Binaries

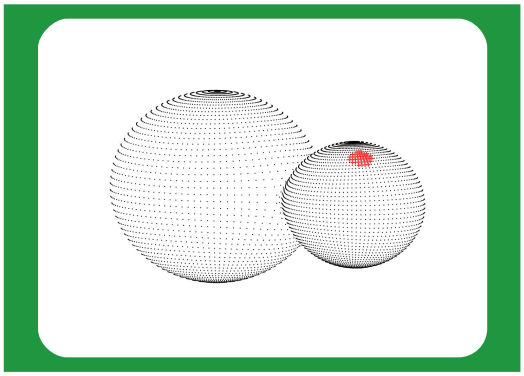

As a starting point, consider visiting the MidnightKite website (http://www.midnightkite.com/index.aspx?URL=Binary) which provides multiple links to a large collection of programs, tutorials, websites, applets and spreadsheets related to the study and modeling of binary stars. If after perusing these sites you still are interested and not intimidated by this field of study, then please read on.

The Roche model derived from the seminal Wilson and Devinney (1971) paper has been widely used to provide synthetic solutions which closely fit light curve changes arising from eclipsing binary star systems. I would strongly recommend purchasing Binary Maker 3 (http://www.binarymaker.com) if you are interested in modeling light curve data (Bradstreet 2005). BM3 comes with a catalog (CALEB) of light curve and radial velocity data from over 300 sample binary systems. These are great teaching tools for the uninitiated astronomer and lay a firm foundation for two other more powerful (but less user friendly) applications which reside in the public domain. The first of these (WDwint) can be downloaded from Bob Nelson's astronomy software website (http://members.shaw.ca/bob.nelson/software1.htm). At the same time you should also download VHLimb which interpolates limb darkening values (van Hamme 1993) which need to be adjusted for each change in effective temperature. This GUI front-end to the Wilson-Devinney (W-D) code can be quirky so carefully read all documentation. In particular make sure that you generally adhere to old-school DOS file and folder naming conventions. They can be longer than 8 characters but no spaces or punctuation except the underscore "_". Prša and Zwitter (2005) released (http://phoebe.fiz.uni-lj.si/?q=node/32) a modern GUI frontend to the W-D code called PHOEBE (Physics Of Eclipsing Binaries) which has been compiled to run on various Linux-, Windows-, and Mac-based systems. Compared to WDwint, PHOEBE is much easier to use due to a simplified data import/entry routine, its implementation of internal van Hamme limb darkening tables and rapid graphical feedback while iterating through various parameter changes. PHOEBE is the best choice after BM3 if you are looking for a higher level of parameter control and importantly, the ability to simultaneously fit more than one light curve acquired with various filters (eg. B, V, R and Ic).

References

Bradstreet, D.H. 2005, "Fundamentals of Solving Eclipsing Binary Light Curves Using Binary Maker 3", Society for Astronomical Sciences, 23.

Ghedini, S. 1981, Societa Astronomica Italiana, 52, 633.

Hamme, W. van 1993, Astron. J., 106, 2096.

Harris, A.W., Young, J.W., Bowell, E., Martin, L.J., Millis, R. L., Poutanen, M., Scaltriti, F., Zappala, V., Schober, H.J., Debehogne, H. and Zeigler, K.W. 1989, Icarus 77, 171.

Kwee, K.K. and Woerden, H. van 1956, B.A.N., 12, 327.

Lenz, P. and Breger, M. 2005, "Period04 User Guide", Comm. in Asteroseismology, 146, 53.

Prša, A., and Zwitter, T. 2005, "A Computational Guide to Physics of Eclipsing Binaries. 1. Demonstrations and Perspectives", Astrophys J., 628, 1, 426.

Wilson, R.E. and Devinney, E.J. 1971, Astrophys J., 166, 605.

Zima, W. 2008, "User Manual for FAMIAS and DAS", Comm. in Asteroseismology, 155, 17.

Photometric Nirvana:

Studying Multiple Variables in the Same FOV

Night skies clear enough to image in New Jersey only occur on a handful of days each month, so that targets need to be carefully selected to maximize the collection of photometric data. This is particularly relevant at UnderOak Observatory (UO) where buildings and trees obstruct the view below 30° altitude and imaging is only possible between 100° and 300° azimuth. Depending on the season and declination this usually amounts to less than 5 hours of tracking a single target. Looking back over the past six years, variable star (period <1 d) campaigns which successfully lead to complete light curves normally lasted between 1 to 2.5 months while minor planet studies (period <0.5 day) were somewhat shorter (3-4 weeks). Most data acquisition is already automated at UO so that the best that could be expected is about 12 objects per year without implementing a different sampling strategy.

Back in 2008 this investigator accidently stumbled onto a largely neglected variable star (KW Peg) that happened to be in the same field-of-view (FOV) as the short period eclipsing binary (BX Peg) which was originally targeted for study. This was a serendipitous catch but I wondered whether there was a way to proactively search for other pairs which fell into the FOV produced by any imaging system. Mathematically it boils down to "what's the distance between two points on a spherical surface" and how does that compare to the optical system FOV? On Earth, the shortest flying distance between two points is commonly called a Great Circle Route whereas on a celestial sphere the relative distance between two objects is known as the angular separation. After a refresher course on spherical geometry (thank you Google), all that was needed was a comprehensive list of variable stars and a spreadsheet program like Excel or the public domain program OpenOffice to perform the heavy math.

The first order of business was to locate an up-to-date listing of variable stars. The "General Catalog of Variable Stars" aka GCVS which is maintained by the Sternberg Astronomical Institute in Moscow, Russia (http://www.sai.msu.su/gcvs/gcvs/index.htm) is the most extensive single source database publically available for variable stars. Specifically, the Combined Table from the General Catalogue of Variable Stars Volumes i-iii, 4th ed. (GCVS4) (Kholopov+ 1988) and the Name-List of Variable Stars Nos. 67-80 p.1 (Kholopov+, 1985-2011) with improved coordinates was used (http://www.sai.msu.su/gcvs/gcvs/iii/iii.dat). Some textual prestidigitation was required to align and cleanup a total of 43,676 separate variable star entries using find/replace and the =LEFT(), =MID(), and =RIGHT() functions after importing into Excel. Quite a few objects (n=159) proved to either be duplicates or devoid of critical data necessary to perform the desired calculations and were therefore eliminated.

The next step was to convert right ascension (RA) and declination (DEC) to degrees for each object using Equations (1) and (2), respectively (Table 1). The decimal equivalents to RA and DEC determined in EQ(1) and EQ(2) must be converted to radians [=RADIANS()] in order for the cosine [cos()] and sine [sin()] functions to work properly in Excel (or OpenOffice). The next formula necessary to complete

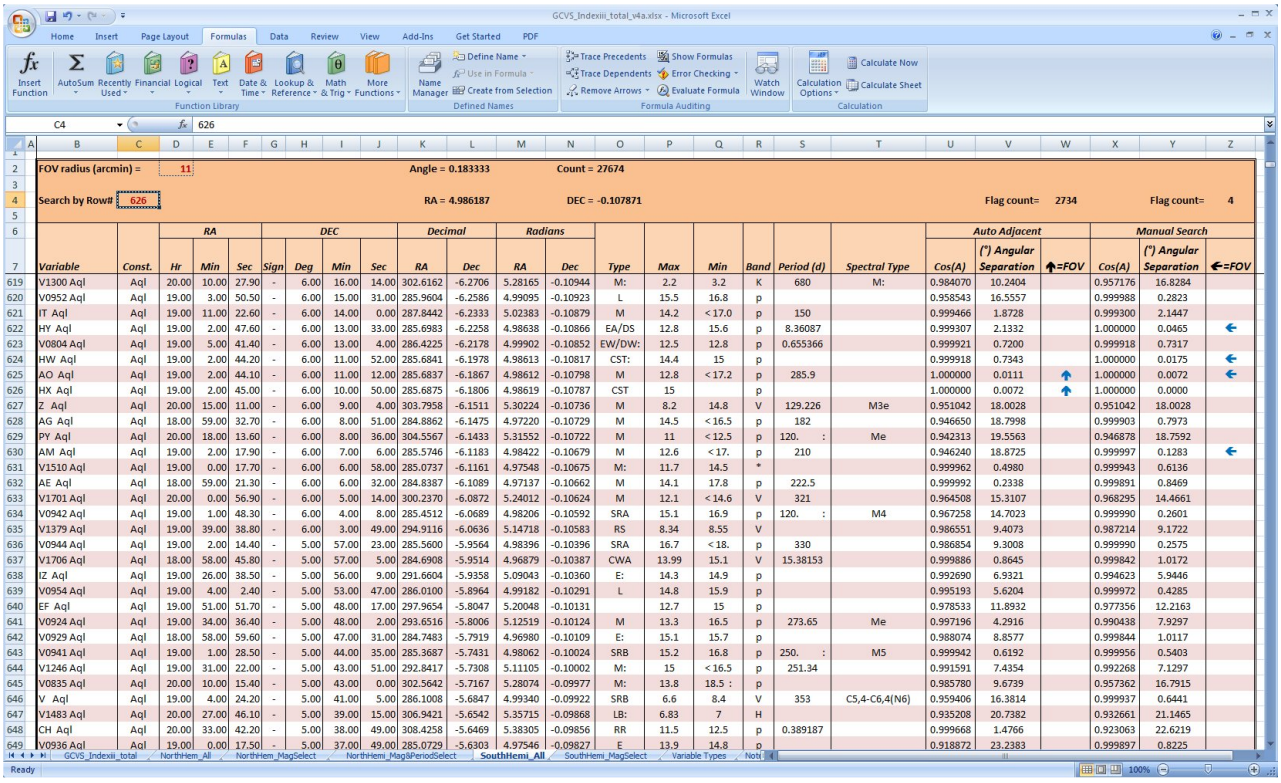

FOV radius (arcmin) = 11 | Angle = 0.183333 | Count = 27674

Search by Row# 626 | RA = 4.986187 | DEC = -0.107871 | Flag count= 2734 | Flag count= 4

	Variable	Const.	RA Hr	RA Min	RA Sec	DEC Sign	DEC Deg	DEC Min	DEC Sec	Decimal RA	Decimal Dec	Radians RA	Radians Dec	Type	Max	Min	Band	Period (d)	Spectral Type	Auto Adjacent Cos(A)	Auto Adjacent (°) Angular Separation	Auto Adjacent ↑=FOV	Manual Search Cos(A)	Manual Search (°) Angular Separation	Manual Search ←=FOV
619	V1300 Aql	Aql	20.00	10.00	27.90	-	6.00	16.00	14.00	302.6162	-6.2706	5.28165	-0.10944	M:	2.2	3.2	K	680	M:	0.984070	10.2404		0.957176	16.8284	
620	V0952 Aql	Aql	19.00	3.00	50.50	-	6.00	15.00	31.00	285.9604	-6.2586	4.99095	-0.10923	L	15.5	16.8	p			0.958543	16.5557		0.999988	0.2823	
621	IT Aql	Aql	19.00	11.00	22.60	-	6.00	14.00	0.00	287.8442	-6.2333	5.02383	-0.10879	M	14.2	< 17.0	p	150		0.999466	1.8728		0.999300	2.1447	
622	HY Aql	Aql	19.00	2.00	47.60	-	6.00	13.00	33.00	285.6983	-6.2258	4.98638	-0.10866	EA/DS	12.8	15.6	p	8.36087		0.999307	2.1332		1.000000	0.0465	←
623	V0804 Aql	Aql	19.00	5.00	41.40	-	6.00	13.00	4.00	286.4225	-6.2178	4.99902	-0.10852	EW/DW:	12.5	12.8	p	0.655366		0.999921	0.7200		0.999918	0.7317	
624	HW Aql	Aql	19.00	2.00	44.20	-	6.00	11.00	52.00	285.6841	-6.1978	4.98613	-0.10817	CST:	14.4	15	p			0.999918	0.7343		1.000000	0.0175	←
625	AO Aql	Aql	19.00	2.00	44.10	-	6.00	11.00	12.00	285.6837	-6.1867	4.98612	-0.10798	M	12.8	< 17.2	p	285.9		1.000000	0.0111	↑	1.000000	0.0072	←
626	HX Aql	Aql	19.00	2.00	45.00	-	6.00	10.00	50.00	285.6875	-6.1806	4.98619	-0.10787	CST	15		p			1.000000	0.0072	↑	1.000000	0.0000	
627	Z Aql	Aql	20.00	15.00	11.00	-	6.00	9.00	4.00	303.7958	-6.1511	5.30224	-0.10736	M	8.2	14.8	V	129.226	M3e	0.951042	18.0028		0.951042	18.0028	
628	AG Aql	Aql	18.00	59.00	32.70	-	6.00	8.00	51.00	284.8862	-6.1475	4.97220	-0.10729	M	14.5	< 16.5	p	182		0.946650	18.7998		0.999903	0.7973	
629	PY Aql	Aql	20.00	18.00	13.60	-	6.00	8.00	36.00	304.5567	-6.1433	5.31552	-0.10722	M	11	< 12.5	p	120. :	Me	0.942313	19.5563		0.946878	18.7592	
630	AM Aql	Aql	19.00	2.00	17.90	-	6.00	7.00	6.00	285.5746	-6.1183	4.98422	-0.10679	M	12.6	< 17.	p	210		0.946240	18.8725		0.999997	0.1283	←
631	V1510 Aql	Aql	19.00	0.00	17.70	-	6.00	6.00	58.00	285.0737	-6.1161	4.97548	-0.10675	M:	11.7	14.5	*			0.999962	0.4980		0.999943	0.6136	
632	AE Aql	Aql	18.00	59.00	21.30	-	6.00	6.00	32.00	284.8387	-6.1089	4.97137	-0.10662	M	14.1	17.8	p	222.5		0.999992	0.2338		0.999891	0.8469	
633	V1701 Aql	Aql	20.00	0.00	56.90	-	6.00	5.00	14.00	300.2370	-6.0872	5.24012	-0.10624	M	12.1	< 14.6	V	321		0.964508	15.3107		0.968295	14.4661	
634	V0942 Aql	Aql	19.00	1.00	48.30	-	6.00	4.00	8.00	285.4512	-6.0689	4.98206	-0.10592	SRA	15.1	16.9	p	120. :	M4	0.967258	14.7023		0.999990	0.2601	
635	V1379 Aql	Aql	19.00	39.00	38.80	-	6.00	3.00	49.00	294.9116	-6.0636	5.14718	-0.10583	RS	8.34	8.55	V			0.986551	9.4073		0.987214	9.1722	
636	V0944 Aql	Aql	19.00	2.00	14.40	-	5.00	57.00	23.00	285.5600	-5.9564	4.98396	-0.10396	SRA	16.7	< 18.	p	330		0.986854	9.3008		0.999990	0.2575	
637	V1706 Aql	Aql	18.00	58.00	45.80	-	5.00	57.00	5.00	284.6908	-5.9514	4.96879	-0.10387	CWA	13.99	15.1	V	15.38153		0.999886	0.8645		0.999842	1.0172	
638	IZ Aql	Aql	19.00	26.00	38.50	-	5.00	56.00	9.00	291.6604	-5.9358	5.09043	-0.10360	E:	14.3	14.9	p			0.992690	6.9321		0.994623	5.9446	
639	V0954 Aql	Aql	19.00	4.00	2.40	-	5.00	53.00	47.00	286.0100	-5.8964	4.99182	-0.10291	L	14.8	15.9	p			0.995193	5.6204		0.999972	0.4285	
640	EF Aql	Aql	19.00	51.00	51.70	-	5.00	48.00	17.00	297.9654	-5.8047	5.20048	-0.10131		12.7	15	p			0.978533	11.8932		0.977356	12.2163	
641	V0924 Aql	Aql	19.00	34.00	36.40	-	5.00	48.00	2.00	293.6516	-5.8006	5.12519	-0.10124	M	13.3	16.5	p	273.65	Me	0.997196	4.2916		0.990438	7.9297	
642	V0929 Aql	Aql	18.00	58.00	59.60	-	5.00	47.00	31.00	284.7483	-5.7919	4.96980	-0.10109	E:	15.1	15.7	p			0.988074	8.8577		0.999844	1.0117	
643	V0941 Aql	Aql	19.00	1.00	28.50	-	5.00	44.00	35.00	285.3687	-5.7431	4.98062	-0.10024	SRB	15.2	16.8	p	250. :	M5	0.999942	0.6192		0.999956	0.5403	
644	V1246 Aql	Aql	19.00	31.00	22.00	-	5.00	43.00	51.00	292.8417	-5.7308	5.11105	-0.10002	M:	15	< 16.5	p	251.34		0.991591	7.4354		0.992268	7.1297	
645	V0835 Aql	Aql	20.00	10.00	15.40	-	5.00	43.00	0.00	302.5642	-5.7167	5.28074	-0.09977	M:	13.8	18.5 :	p			0.985780	9.6739		0.957362	16.7915	
646	V Aql	Aql	19.00	4.00	24.20	-	5.00	41.00	5.00	286.1008	-5.6847	4.99340	-0.09922	SRB	6.6	8.4	V	353	C5,4-C6,4(N6)	0.959406	16.3814		0.999937	0.6441	
647	V1483 Aql	Aql	20.00	27.00	46.10	-	5.00	39.00	15.00	306.9421	-5.6542	5.35715	-0.09868	LB:	6.83	7	H			0.935208	20.7382		0.932661	21.1465	
648	CH Aql	Aql	20.00	33.00	42.20	-	5.00	38.00	49.00	308.4258	-5.6469	5.38305	-0.09856	RR	11.5	12.5	p	0.389187		0.999668	1.4766		0.923063	22.6219	
649	V0936 Aql	Aql	19.00	0.00	17.50	-	5.00	37.00	49.00	285.0729	-5.6303	4.97546	-0.09827	E	13.9	14.8	p			0.918872	23.2383		0.999897	0.8225	

Figure 1.
Snapshot of customized GCVS spreadsheet showing a sampling of variable stars in Aquila sorted by declination.

the calculation of angular distance (A) between two stars is EQ(3), where d_1 is the declination in degrees for star1, d_2 is the declination for star2, ra_1 is the right ascension in degrees for star1 and ra_2 is the right ascension for star2. Again, in order for the spreadsheet to properly calculate EQ(3) all degrees must be converted to radians. Finally, the "(°) angular separation" for each pair was calculated using EQ(4).

The combined GCVS tables and name-lists were divided into separate Northern (-10 to 90° Dec) and Southern (+10 to -90° Dec) object sheets to simplify management of the database. This also minimized the possibility of false negatives during the search for adjacent entries which fall within each defined FOV (more about this later). An example from the Southern Hemisphere sheet that has been sorted by constellation, Dec, and then RA is shown above (Fig. 1) for a grouping of variables in Aquila.

Only a single value, which is in essence a search radius, is required to find potential variable stars clustered within the same FOV. Based upon the ST-402ME camera chip size (4.6 x 6.9 mm) as well as the aperture (200 mm) and focal length (1800 mm) of a Vixen VC200L telescope, the field of view produced by this optical system is 8.8 x 13.1 arcmin. In this case the average dimension (~11 arcmin or 0.18333°) seemed to be a reasonable compromise and when entered into the spreadsheet (D2) resulted in over

Table 1. Critical Formulae

(1) Deg_{RA} = (RA_hours × 15) + (RA_minutes × 0.25) + (RA_seconds × 0.004166)
(2) Deg_{DEC} = [ABS(DEC_degrees) + (DEC_minutes/60) + (DEC_seconds/3600)] × SIGN (DEC_degrees)]
(3) cos (A) = sin (d_1) × sin (d_2) + cos (d_1) × cos(d_2) × cos (ra_1-ra_2)
(4) Angular separation = ACOS((value))*(180/pi())).

2700 hits! However, it must be pointed out that this also includes stars as faint as 20 mag which is far beyond the light trapping ability of an 8" telescope. More practically, when the magnitude range was narrowed between 8.5 and 13.5 (any star brighter than 8.5 will quickly saturate the detector), then at least 800 stars still had variable companion(s) which could be detected in the same FOV. Further refinement to only include variables with regular periods under 20 days diminished the number of candidates to less than 200 objects. The automatic search algorithm depends upon sequential adjacencies produced after sorting the list. Each cell in the Cos(A) column looks at the cell above to determine whether this pairing falls within the FOV of the optical train. If true, then that star is flagged with an upwards arrow which points to its FOV companion. This search appears to operate most effectively when each list is sorted by constellation name, declination and right ascension.

A blowup of the previous search output is shown below (Fig. 2). In this case three stars (HX Aql, AO Aql and HW Aql) are all within the same FOV. HX Aql is separated by 0.0072° from AO Aql and AO Aql is separated from HW Aql by 0.0111°. The "auto adjacent" search is fairly primitive and fails by itself in congested regions of the sky (eg Milky Way and star clusters). Sorting does not guarantee that all possible candidate stars are grouped consecutively so a separate manual search mode (Search by row#) was designed to address this possibility. In the above example HX Aql is located in row 626 so that entering this number into cell C4 will force a row-by-row search to identify all instances where the search criterion is met. Two additional stars (HY Aql and AM Aql) were flagged (left-pointing arrow) as partners in what is now a five-some. Indeed as shown in Fig. 3, all five stars neatly fit in the same FOV reproduced using the imager context viewer in SkyTools 3 Pro.

It should be noted that with the constellation-Dec-RA sorting strategy, when an object of interest is located on the border between two or more constellations, a manual search is the only way to ensure that all possibilities are captured. Feel free to try other sort combinations which might improve the flag count for

FOV radius (arcmin) = 11

Search by Row# 626 Flag count= 2734 Flag count= 4

		RA		Auto Adjacent			Manual Search		
Variable	Const.	Hr		Cos(A)	(°) Angular Separation	↑=FOV	Cos(A)	(°) Angular Separation	←=FOV
V1300 Aql	Aql	20.00	....	0.984070	10.2404		0.957176	16.8284	
V0952 Aql	Aql	19.00	....	0.958543	16.5557		0.999988	0.2823	
IT Aql	Aql	19.00	....	0.999466	1.8728		0.999300	2.1447	
HY Aql	Aql	19.00	....	0.999307	2.1332		1.000000	0.0465	←
V0804 Aql	Aql	19.00	....	0.999921	0.7200		0.999918	0.7317	
HW Aql	Aql	19.00	....	0.999918	0.7343		1.000000	0.0175	←
AO Aql	Aql	19.00	....	1.000000	0.0111	↑	1.000000	0.0072	←
HX Aql	Aql	19.00	....	1.000000	0.0072	↑	1.000000	0.0000	
Z Aql	Aql	20.00	....	0.951042	18.0028		0.951042	18.0028	
AG Aql	Aql	18.00	....	0.946650	18.7998		0.999903	0.7973	
PY Aql	Aql	20.00	....	0.942313	19.5563		0.946878	18.7592	
AM Aql	Aql	19.00	....	0.946240	18.8725		0.999997	0.1283	←
V1510 Aql	Aql	19.00	....	0.999962	0.4980		0.999943	0.6136	
AE Aql	Aql	18.00	....	0.999992	0.2338		0.999891	0.8469	
V1701 Aql	Aql	20.00		0.964508	15.3107		0.968295	14.4661	

Figure 2.
Blowup of spreadsheet showing the results from an automatic adjacent and a manual row-by-row search for variable stars clustered around HX Aquilae

stellar cohorts in the same FOV.

In summary, this spreadsheet which is posted at (www.underoakobservatory.com/GCVS_FOVar_UO_Issue2.xlsx) can be used to intentionally target an area where more than one variable star will fall into a defined FOV. Proactively collecting light curve data from more than one variable star during the same session may be an attractive approach in regions of the world where weather limits the number of clear nights. Secondly, and perhaps equally important, the unmodified database can be used to identify variables around target(s) which might unintentionally be used as fixed-magnitude comparison or check stars during photometric reduction to relative flux or magnitudes.

Reference

Samus N.N., Durlevich O.V., Kazarovets E V., Kireeva N.N., Pastukhova E.N., Zharova A.V., et al. General Catalog of Variable Stars (GCVS database, Version 2011 Jan), CDS B/gcvs.

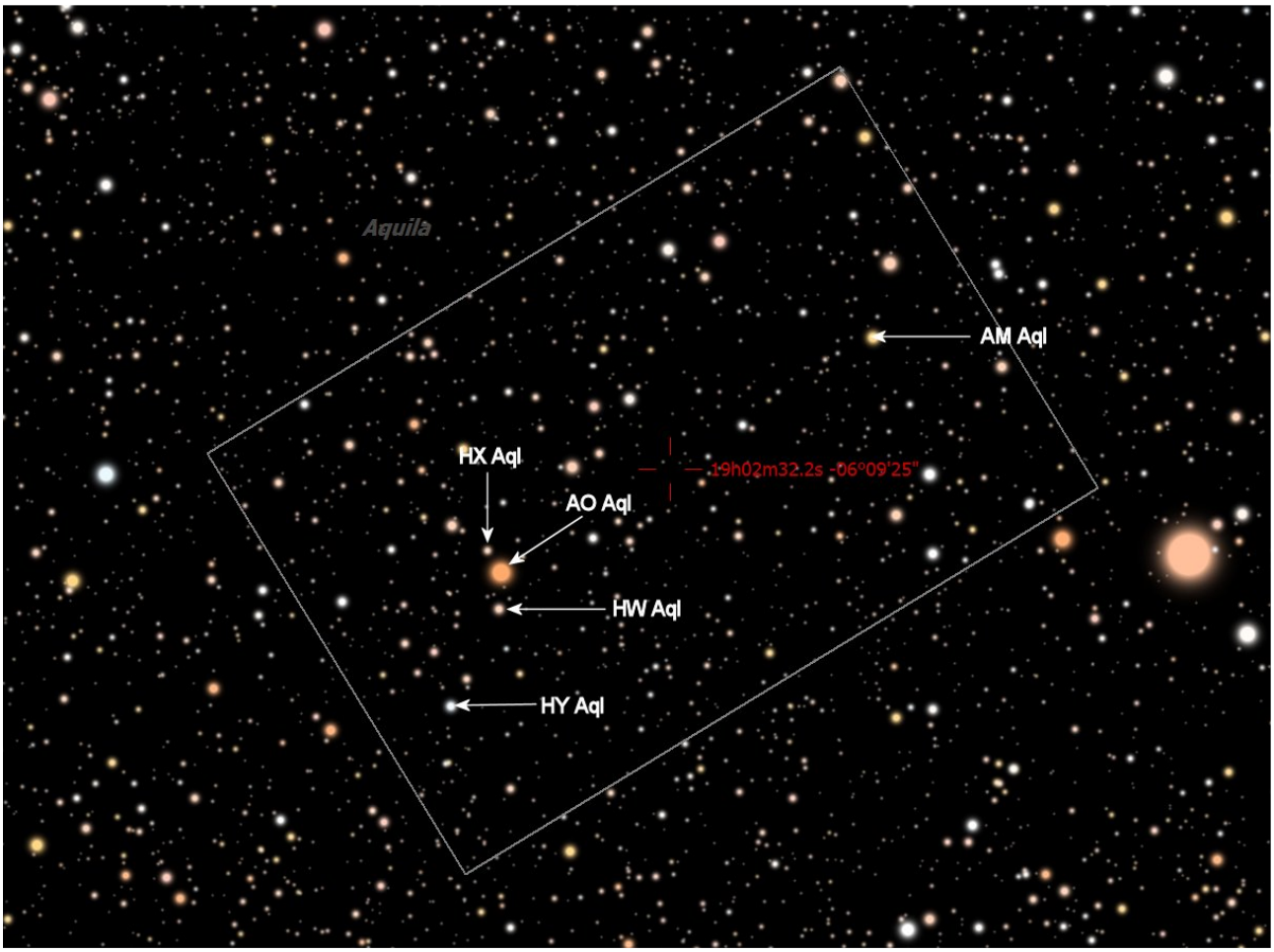

Figure 3.
Simulated FOV (8.8 x 13.1 arcmin) for VC200L @f/9 coupled with an SBIG ST-402ME ccd camera. Image was rendered using the context viewer in SkyTools 3 Pro and shows 5 known variable stars which would be captured in a single image.

Research Article

CCD Photometric and Period Analysis of RT LMi, a W UMa Type Eclipsing Binary With a Split Personality

Abstract

RT LMi is an overcontact W UMa binary system for which there has been significant ambiguity in the literature regarding its classification (A- or W-subtype). This rapidly rotating (P=0.374917 d) eclipsing binary was investigated at UnderOak Observatory to better understand the uncertain behavior of this variable. Photometric data collected in three bandpasses (B, V and I_c) produced 7 new times-of-minima which were used to update the linear ephemeris and further analyze secular changes in orbital periodicity. In addition, modeling of the Roche geometry was accomplished with the assistance of three different programs which employ the Wilson-Devinney code. Overall, results from the present study provide a strong case for a unified W-subtype Roche model solution to all published light curves. The primary minimum for RT LMi results from the transit of a smaller but slightly hotter secondary across the face of the primary star while the flat-bottomed secondary minimum indicates that the cooler primary companion completely occults its smaller cohort.

1. Introduction

W UMa-type variable stars belong to a class of overcontact eclipsing binaries whose component main sequence stars (spectral type A–F to early K) rotate rapidly (P<1 d). Since its discovery by Hoffmeister (1949), refined photoelectric (pe)- or CCD-derived light elements for RT LMi have been reported by Hoffman and Meinunger (1983), Hoffmann (1984), Niarchos et al (1994), Yang and Liu (2004), Qian et al (2008), and Zola et al (2010). A radial velocity study was conducted by Ruciński et al (2000) which yielded a spectroscopic mass ratio value (q_{sp}=0.376) for this binary system. RT LMi consists of two main sequence stars; the primary constituent has been variously reported between F7V and G0V spectral classes. Based solely upon the radial velocity data from Ruciński et al (2000), RT LMi belongs to the A-subtype classification since the more massive rather than its less massive companion is eclipsed at primary minimum. Typically with A-subtype W UMa systems, the temperature of the primary star is somewhat higher than the secondary. This is in contrast to an earlier investigation (Niarchos et al 1994) where a W-subtype configuration was assigned albeit based upon a photometrically derived q_{ph}-value (2.5943) which is very close to the reciprocal of the spectroscopically derived q_{sp} (0.376) published six years later. Yang and Liu (2004) describe in some detail the peak asymmetry at maximum light often called the O'Connell effect and commonly observed with W UMa variables. Their light curves collected in 2003 exhibited a positive O'Connell effect (Max I> Max II) whereas the 1982 light curve from Hoffmann (1984) showed a negative O'Connell effect. In addition, Yang and Liu (2004) reported that the difference in minimum light (Min I - Min II) also varied between studies. Both investigators resorted to the addition of cool or hot starspots in order to obtain the best light curve fits with Roche modeling. The ostensibly symmetrical light curves published by Qian et al (2008) add to the uncertainty regarding the W UMa classification of RT LMi. They argue that even though the shape of the light curve at primary minimum meets the Binnendijk (1970) definition for an A-subtype system, the best synthetic Roche model solution is achieved when the effective temperature of the less-massive star (T_2) is higher than the more-massive constituent (T_1). Interestingly, this situation (T_2>T_1) is a defining characteristic for a W-subtype system and further adds to the ambiguity in characterizing this chameleon-like binary. The orbital inclination angle is remarkably similar (~83.5°) in all studies where it has been reported such that our view of this eclipsing binary is very close to edge-on. In addition, all evidence accumulated thus far precludes the possibility of a third body which gravitationally influences this system.

2. Observations and Data Reduction

2.1. Astrometry

Images of RT LMi were automatically matched against the standard star fields (UCAC3) provided in MPO Canopus (V10.3.0.2, Minor Planet Observer 2010) and then rotated and scaled as necessary. Plate constants were internally calculated which convert X/Y coordinates of a detected object to a corresponding RA and declination.

2.2. Photometry

CCD photometric measurements began on March 30, 2008 and finished 9 sessions later on May 30, 2008. Equipment included a 0.2-m Schmidt-Cassegrain telescope (f/6.3) with an SBIG ST-402ME CCD camera mounted at the primary focus. Automated multi-bandwidth imaging was performed with SBIG photometric B, V and I_c filters manufactured to match the Bessell prescription. Typical image acquisition parameters, exposure (50 sec), and data reduction (lights, darks and flats) for this optical system have been described in detail by Alton (2009). Instrumental readings were reduced to catalog-based magnitudes using the MPOSC3 reference star fields built into MPO Canopus. Accurate timing for each image is critical; therefore the computer clock was updated via the Internet Time Server immediately prior to each session. Image acquisition (raw lights, darks, and flats) was performed using CCDSoft 5 while calibration and registration were accomplished with AIP4Win (V2.3.1, Berry and Burnell 2008). MPO Canopus provided the means for further photometric reduction (differential instrument magnitudes) using two non-varying comparison stars to ultimately calculate ephemerides and orbital period.

2.3 Light Curve Analyses

Roche type modeling was performed using Binary Maker 3 (Bradstreet and Steelman 2002), PHOEBE (Prša and Zwitter 2005) and WDwint5.6a (Nelson 2009), all of which employ the Wilson-Devinney (W-D) code (Wilson and Devinney 1971; Wilson 1979). WDwint (http://members.shaw.ca/bob.nelson/software1.htm) and PHOEBE (http://phoebe.fiz.uni-lj.si/) are freely available GUI implementations of the W-D model. 3-D renderings of RT LMi were also produced by Binary Maker 3 once each model fit was finalized.

3. Results and Discussion

3.1. Photometry

There were only two stars bright enough (B mag) in the same FOV with RT LMi to calculate the relative change in flux and derive catalog-based (MPOSC3) magnitudes using the "Comp Star Selector" feature in MPO Canopus (Table 1). Comparison stars cannot vary at least over each observation session to successfully apply differential photometry. The difference in magnitude over time from each comparison star against the averaged magnitude yielded a narrow range of values with no obvious trend. In this case variability was generally within ±0.015 mag for V and I_c filters and ±0.03 for B passband. Images were only taken above 30° altitude (airmass = 2.0) thereby minimizing error due to differential refraction and color extinction.

3.2. Ephemeris

Photometric values in B (n=745), V (n=758), and I_c (n=760) passbands were combined by filter and folded to produce light curves that spanned 8 weeks of imaging (Fig. 1). These observations included 7 new times-of-minima (ToM) in each bandpass. Initially seeded with the orbital period posted by Kreiner (2004) at the Mt. Suhora Astronomical Observatory

Table 1. Astrometric coordinates (J2000) and MPOSC3 catalog magnitudes (V, B and I_c) for two comparison stars used in this photometric study

Star Identification	R.A.	DEC	MPOSC3 V mag	MPOSC3 B mag	MPOSC3 I_c mag
T. RT LMi	09:49:48.3	+34:27:15	(11.32-11.93)[a]	(11.86-12.47)	(10.68- 11.3)
1. TYC 02505-00791	09:49:31.8	+34:33:24	10.27	10.96	9.51
2. J094950.4+342505	09:49:50.4	+34:25:05	13.04	13.87	12.15

a: Range of magnitudes for RT LMi from present study

website (http://www.as.up.krakow.pl/ephem/lmi.htm), the Fourier analysis routine in MPO Canopus provided a period solution for all the data. The time-of-minimum for the latest primary epoch was estimated using the Hertzsprung method as detailed by Henden and Kaitchuck (1990); the corresponding linear ephemeris equation (1) was determined to be:

Min I (hel.) = 2,454,555.5643 + 0.3749170 (1) E (1)

This orbital period compares very favorably with modern values reported over the past 3 decades and was independently confirmed (PERANSO v 2.5, CBA Belgium Observatory) by applying periodic orthogonals (Schwarzenberg-Czerny 1996) to fit observations and analysis of variance (ANOVA) to evaluate fit quality.

ToM values were estimated by MINIMA (V25b; Nelson 2007) using a simple mean from a suite of six different methods including parabolic fit, tracing paper, bisecting chords, Kwee and van Woerden (1956), Fourier fit, and sliding integrations (Ghedini 1981). Five new secondary (s) and two new primary (p) minima were recorded during this investigation. No meaningful color dependencies emerged; therefore the timings from all three filters were averaged for each session (Table 2). These seven minima along with additional values published at the AAVSO, IBVS, VSOLJ, and B.R.N.O. websites were used to update the RT LMi "Eclipsing Binary O-C" EXCEL spreadsheet file developed by Nelson (2005b) and last revised with 2010 values. The reference epoch (Kreiner 2004) used to calculate O-C residuals was defined by the following linear ephemeris equation (2):

Min I (hel.) = 2,452,500.2081 (1) + 0.37491744 (3) E (2)

The "observed minus calculated" (O-C) data are limited to a composite (n=70) photographically derived value determined in 1957, two pe values in 1982, and 70 other observations (pe and ccd) collected since 1994 (Fig. 2). Two recent papers, both of which used an even smaller dataset, proposed a 47 (Qian et al 2008) or 64 (Yang and Liu 2004) year sinusoidal period for this system which they attributed to magnetic activity cycles (Applegate 1992) rather than third light. As can be clearly seen in the O-C diagram for RT LMi (Fig. 2), any period analysis would have to assume that the last 20 years of photometric data are representative of the behavior of this system since the first O-C value was recorded. According to the Nyquist theorem, the sampling frequency should be at least twice the highest frequency contained in the signal. Since 20 years is only one-third to one-half the duration of the two aforementioned cycles, these estimates are fraught with potential aliasing or false signals, and need to be viewed with great caution. With these caveats in mind, a new non-linear regression analysis using a scaled Levenberg-Marquardt algorithm was performed (QtiPlot v0.9.8; http://soft.proindependent.com/qtiplot.html) on the updated dataset. A quadratic equation (3) modulated with a sine term produced a reasonable fit (r^2>0.92) of the O-C versus cycle number data.

Table 2. New times of minimum for RT LMi collected at UnderOak Observatory

Computed Time of Minimum (HJD–2400000.0)	*ToM ±Error*	*UT Date of Observations*	*Type of Minimum*
54569.56561	0.0002	13April2008	s
54572.56537	0.0002	16April2008	s
54575.56417	0.0004	19April2008	s
54578.56393	0.0003	22April2008	s
54581.56291	0.0004	25April2008	s
54586.62394	0.0003	30April2008	p
54616.61743	0.0003	30May2008	p

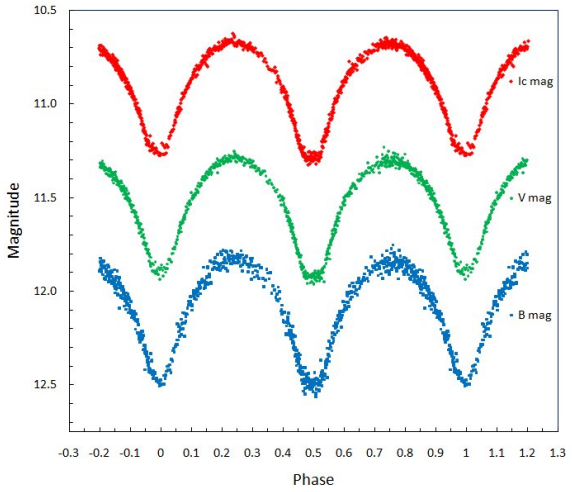

Figure 1.
Folded CCD-derived light curves for RT LMi collected between March 30 and May 30, 2008. The top (I_C), middle (V) and bottom (B) curves shown above were analyzed using MPO Canopus and reduced to magnitudes from the MPOSC3 catalog.

$$c + a_1{*}x + a_2{*}x^2 + a_3{*}\sin(a_4{*}x + a_5) \quad (3)$$

Accordingly, the coefficients (±error) for each solved term in the above expression are provided in Table 3. From the parabolic component ($c + a_1{*}x + a_2{*}x^2$) it is apparent that the orbital period has been slowly decreasing linearly with time as suggested by the negative coefficient (a_2) for the quadratic term, x^2. This solution leads to the following quadratic ephemeris equation (4):

$$\text{Min I (hel.)} = 2455275.3482\ (2) + 0.37491758\ (5)\ E - 7.031\ (1.09)\times10^{-12}\ E^2 \quad (4)$$

Commonly observed in W UMa binary systems, secular orbital period changes may be associated with material transfer between the secondary and primary component. The orbital period linear rate of decrease since 1957 can then be defined by the equation (5) below:

$$dP/dt = 2\times(-7.031\times10^{-12})\ (1/0.37491758)\ (86400)\ (365.25) = -0.00118\ \text{sec/yr} \quad (5)$$

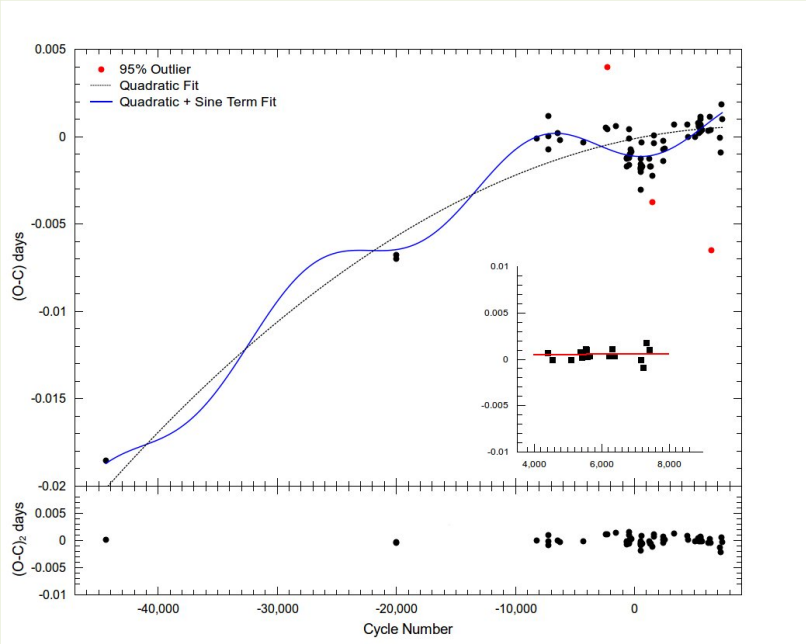

Figure 2.
Non-linear regression fit of photoelectric and CCD time-of-minimum observations (1957-2010) using a quadratic expression modulated with a sine term (top panel). The inset graph shows a straight-line segment of data from 2007 to 2010 used to calculate a near term linear ephemeris for RT LMi. The bottom panel shows $(O-C)_2$ residuals after the sine modulated quadratic fit of data.

Light Curve Diagnostics

The appearance of a flat-bottomed minimum in an eclipsing binary light curve is highly diagnostic for two physical attributes of the system. Before getting into the details, let's review the definitions for eclipse, transit and occultation as they relate to binary stars. The movements of two stars in a binary system lie in a common plane. Any detector aligned very closely with this plane, will see both stars pass in front of each other. An occultation occurs when a larger body passes in front and completely hides an apparently smaller body. In contrast, a transit involves the movement of a smaller body across the face of an apparently larger body. An eclipse is a more general term which describes the action of one body passing in front of another which can result in totally obscuring or partially hiding the object. A photometric detector records the changing luminosity associated with each occultation, transit or eclipse and accordingly produces a light curve with two minima during one orbital period. A flat-bottomed minimum typically results from occultation of the smaller constituent by the larger companion. The extent and duration of the flat portion depends on the size difference and the angle of inclination (i). Let's look at these two situations separately.

The angle of inclination can range between 0 to 90° from the viewer's perspective. A view from the top of the binary system occurs at 0° while the best vantage point for investigation is exactly edge-on or at 90°. The effect on the flat-bottomed shape of the minimum resulting from an occultation is fairly dramatic between an inclination angle of 80 and 90°. This can be seen in the simulated light curve from a contact binary system below (Fig. A1). In this example, Min I corresponds to the transit of a cooler secondary across the face of the primary at phase 0, whereas Min II is associated with the occultation of the secondary by the hotter primary star (Fig. A2). The spatial orientation at phase = 0.5325, rather than 0.5, was selected to ensure that differences could actually be seen at all four inclination angles.

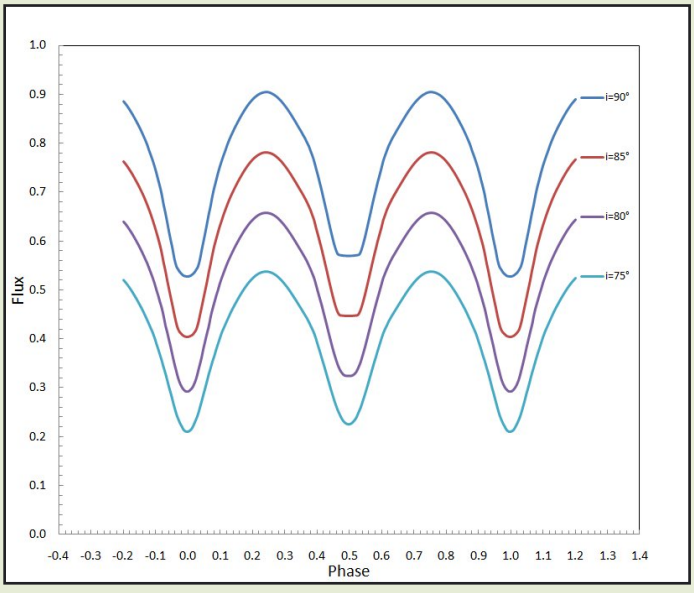

The effect that the comparative size of each star in a binary system has on a light curve is no less subtle than that observed with changes in the angle of inclination. A series of light curves were simulated by fixing i (90°) and changing the mass ratio ($q = m_2/m_1$) of component stars to values ranging between 0.2 and 0.5 (Fig. B1). These correspond to systems in which the mean radius ratio (r_1/r_2) varies from 1.36 to 2.06 when the degree of contact was maintained at a constant value (f≈0.17 or 17% overlap). The width of each minimum increases as the difference in size between binary components becomes greater (Fig. B2); Min II takes on a decidedly flattened shape.

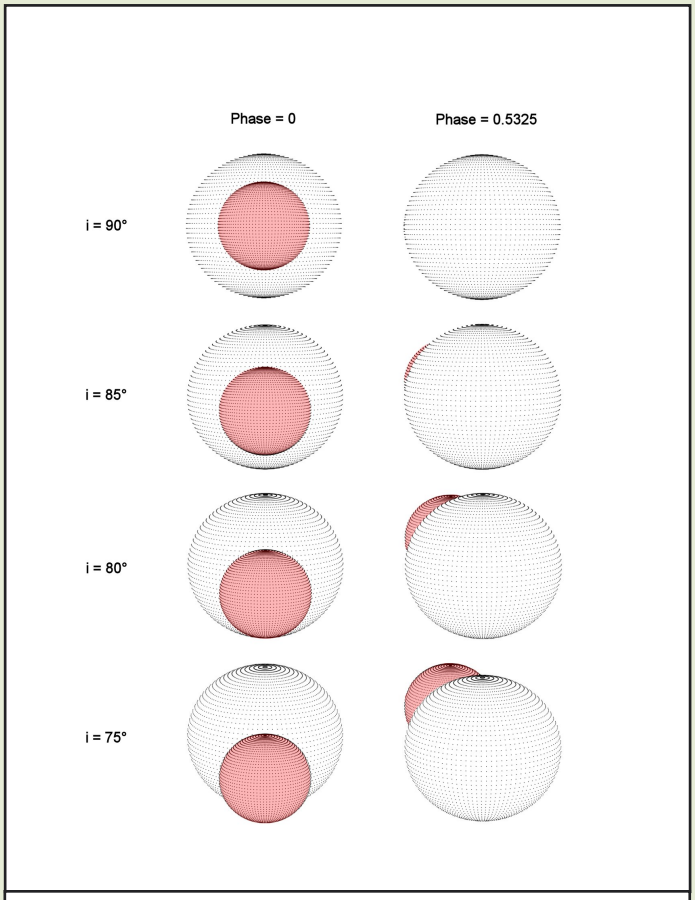

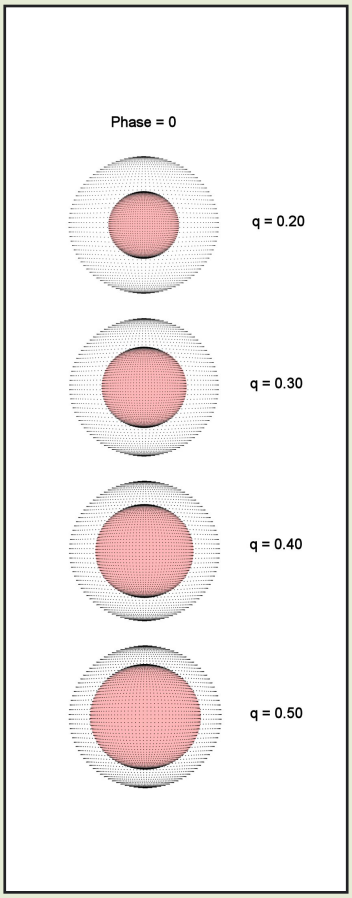

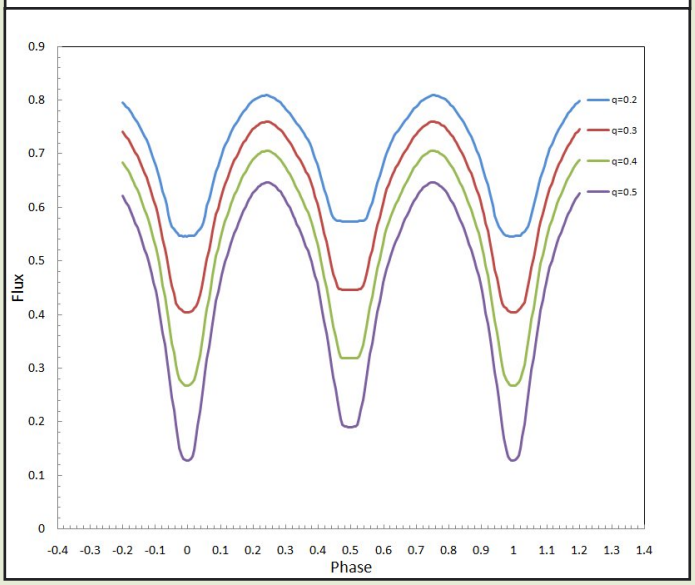

Figure A1. Change in light curve shape with decreasing angle of inclination (opposing page)

Figure A2. Spatial view of binary system during Min I and at phase = 0.5325 (top left)

Figure B1. Change in light curve shape with star size differential (bottom left)

Figure B2. Spatial view of binary system during Min I (top right) with varying q (m_2/m_1)

Table 3. Coefficients from non-linear regression fit of O-C data for RT LMi

c	a_1	a_2	a_3	a_4	a_5
1.433×10^{-5} (1.78)	1.441×10^{-7} (0.468)	-7.031×10^{-12} (1.09)	1.430×10^{-3} (0.183)	3.290×10^{-4} (0.347)	4.249 (0.227)

The first modern period (0.3749180 d) for RT LMi was determined by Hoffmann and Meinunger (1983). The linear ephemeris from the present investigation was predicted from a straight line segment (Fig. 2 inset) covering near-term observations from 2007 to 2010. The revised period (Eq 6) is also consistent with an overall decrease in orbital period:

Min. I (hel.) = 2,455,275.3476 (8) + 0.37491747 (14) E (6)

New ephemerides for RT LMi should be calculated on a regular basis due to the complex changes in orbital period for this system. Any claim regarding the cyclical behavior of this system is heavily influenced by photometric observations collected over the relatively short time since 1994 (cycle -8225.5). The amplitude (0.001430) of the periodic oscillation is defined by the coefficient of the sine term (a_3), while the period of the sinusoidal oscillations was calculated according to the relationship:

$$P_3 = 2\pi P/\omega, \quad (7)$$

where ω, the angular frequency, is defined by a_4. The sinusoidal period estimated from Eq (7) was 19.6 yr and more in line with changes in magnetic activity and spot formation commonly observed (18-20 yr) in other W UMa binary systems (Borkovits et al 2005). By comparison, much longer periods (47-64 yr) were proposed by Yang and Liu (2004) and Qian et al (2008). Both groups suggested that a light-time-effect produced by the gravitational influence of a third body could account for similar sinusoidal oscillations but largely discounted this possibility due to lack of independent supporting evidence. A spectroscopic search by D'Angelo et al (2006) also failed to uncover a faint tertiary companion for RT LMi.

3.3 Light Curve Synthesis

Individual light curves (Fig. 1) show that minima are separated by 0.5 phase and therefore consistent with a circular orbit. Similar to the light curves reported by Zola et al (2010), near symmetry was observed at maximum light (Max I=Max II). This is in contrast to the 1982 (Niarchos et al 1994) and 2003 (Yang and Liu 2004) light curves which revealed a negative (Max II>Max I) and positive (Max I>Max II) O'Connell effect, respectively. The O'Connell effect is believed to involve the presence of cool starspot(s), hot regions, gas stream impact on one of the binary components, or other unknown phenomena which distort surface homogeneity and can produce unequal heights during quadrature (Yakut & Eggleton 2005). Light curves from this 2008 study exhibit unequal depths at minimum light which are consistent with that observed by Yang and Liu (2004). Special mention, however, should be made regarding the phase assignment of the 2008 deepest minima in Fig. 1 and the flat-bottomed shape which is similar to that reported by Niarchos et al (1994). Careful examination of the new times of minima (Table 1) reveals that the deepest minima are actually the secondary minima. Furthermore, it is also conceivable that Niarchos et al (1994) incorrectly assigned the primary minimum for the 1982 light curve; only two times-of-minima were reported and both minima had nearly the same intensity. The potential mis-assignment of minima by Niarchos et al (1994) and the new light curve described herein have a direct bearing on the A- and W-subtype duality often ascribed to this binary system in the literature. Based upon the low mass ratio (q_{sp}=0.366), and high angle of inclination (~83.5°), the expectation is that Min II would be flat-bottomed. This effect is consistent with that observed for RT LMi during the 2008 campaign (Fig. 1).

Roche modeling of RT LMi with PHOEBE employed Mode 3 (an overcontact binary system not in thermal contact) with synchronous rotation and circular orbits. Each model fit of data from the present study incorporated individual observations assigned an

equal weight of 1. Bolometric albedo ($A_{1,2}$=0.5) and gravity darkening coefficients ($g_{1,2}$=0.32) for cooler stars with convective envelopes were assigned according to Ruciński (1969) and Lucy (1967), respectively. Following any Teff change to either star, new logarithmic limb darkening coefficients (x_1, x_2, y_1, y_2) were interpolated within PHOEBE according to Van Hamme (1993). The effective temperature (Teff) of the primary was estimated from the B-V magnitude determined during Min II when the primary occults the secondary and its spectral output is least contaminated. Since W UMa systems are invariably comprised of main sequence stars, the mean dereddened (E_{B-V} = 0.011) value for B-V (0.573) corresponds to an effective temperature of ~6000 °K (Flower 1996). Other investigators (Niarchos et al 1994, Awadalla and Hanna 2005 and Ruciński et al 2000) report that the spectral type of RT LMi ranges between G0 (5943 °K) and F7V (6270 °K), although the latter group did point out that their spectral classification (F7V) was based on poor spectra. The SIMBAD astronomical Database (http://simbad.u-strasbg.fr/simbad/) lists RT LMi as F7V. Due to the ambiguity in classifying the subtype (A or W) of this W UMa system a number of different temperature combinations (5800 – 6400 °K) for both stars were investigated.

3.4 Roche Modeling

3.4.1 A-Subtype

Based strictly upon radial velocity studies (Ruciński et al 2000), RT LMi conforms to the A-subtype where the most massive and hotter star is eclipsed at primary minimum. Accordingly, their most recent mass ratio value (q_{sp}=0.366) and those for $\Omega_{1,2}$ (2.57) and i (84.1°) reported by Qian et al (2008) were adopted as a starting point for an unspotted A-subtype (T_1>T_2) fit using the commercial application Binary Maker 3 (BM3). Initial attempts with T_1 fixed at 6000 °K (G0V) involved iteratively adjusting the effective temperature of the secondary (T_2), orbital inclination (i), limb-darkening (x_1 and x_2; linear-cosine) and common envelope surface potential (Ω_1=Ω_2) until a reasonable fit of the model to normalized flux (V) was obtained. Model fitting in PHOEBE employed phased data which had been transformed into catalog-based magnitudes. A_1, A_2, g_1, g_2, and T_1 were fixed parameters whereas $\Omega_{1,2}$, T_2 (initial value = 5800 °K), phase shift, x_1, x_2, y_1, y_2, and i were iteratively adjusted while applying differential corrections (DC) to achieve a simultaneous minimum residual fit of all (B, V, and I_c) photometric observations. Even though the mass ratio (q_{sp}=0.366) was established from radial velocity data (Ruciński et al 2000), the authors of this paper did reveal that this value was based on poor spectra. Thereafter, q was also allowed to vary while seeking a solution to the Roche model. Starting with a no-spot model in PHOEBE, the initial values from BM3 converged to a new solution which significantly underestimated Min II (Fig. 3). The possibility therefore exists that the introduction of a starspot could address this disparity in the model fit. RT LMi Light curves from four previous investigations were closely examined for some hint as to whether a cold spot is more likely than a hot spot or whether the primary as opposed to the secondary star is affected. Phased light curve data (Δ mag) which were tabulated in the papers by Yang and Liu (2004) and Qian et al (2008) were converted to flux according to the expression:

$$\text{Flux} = 10^{-0.4\times\Delta\text{mag}}$$

and then normalized such that the highest intensity =1; this allowed direct comparison of light curves from five different epochs (1982, 2001, 2003, 2005 and 2008). Aside from a slightly elevated Max I in the rephased light curves generated by Niarchos et al (1994), the difference in flux between Max I and Min I was fairly constant (0.41 – 0.42) amongst all the others. Most of the variability was associated with Min II and Max II, so that starspot(s) were positioned to address these observed differences. The present study simultaneously achieved a model fit in three colors (B, V and Ic); elements for RT LMi obtained with a cold spot on the primary star using PHOEBE are provided in Table 4. Light curve fits are reproduced in Figs. 4 (I_c mag), 5 (V mag), and 6 (B mag) while a 3-dimensional spatial model for RT LMi invoking a cool spot on the primary is shown in Fig. 7. The short term oscillations (~19.6 yrs) suggested by the O-C diagram are consistent with the existence of starspot(s), however, as mentioned previously, it is also possible that an unrelated mechanism is involved in perturbing the light curve for this binary system.

Since phase vs RT LMi intensity data were published

in toto by Niarchos et al (1994), Yang and Liu (2004), and Qian et al (2008), new A-subtype modeling was also performed on these light curves. For consistency, values for T_1 (6000 °K) and the mass ratio (0.381) which led to good fits of the 2008 light curves acquired at UnderOak Observatory were initially held constant while iteratively adjusting the effective temperature of the secondary, inclination (i), and common envelope surface potential ($\Omega_{1,2}$) until an acceptable fit of the model to normalized flux was obtained such that $T_1 > T_2$. A comparison of light curve parameters and geometric elements obtained from Roche modeling is summarized in Table 4. The corresponding fits to each model are shown in Fig. 8 (Niarchos et al 1994), Fig. 9 (Yang and Liu 2004) and Fig. 10 (Qian et al 2008). Curiously, Qian et al (2008) argue that maximum light exhibits symmetry and minima show "near similar depth" for their light curve collected in 2001, yet this is quite contrary to the results after plotting (Fig. 10) the normal photometric data which they published in tabular form. Assuming that these binned data are an accurate reflection of the raw dataset (n=4325 time points), a spotted model was necessary to best fit these data since they clearly show that Max I>Max II and Min I>Min II. Light curve data from Zola et al (2010) were not in the public domain at the time this document was being prepared and therefore could not be modeled for a potential A-subtype solution. Nonetheless, solutions for the four tabulated epochs shared reasonably similar values for

Table 4. A Comparison of Selected Geometrical and Physical Elements for RT LMi Obtained Following Roche Model Light Curve Fitting as an A-subtype W UMa Binary System

Parameter	Present Study	Niarchos et al (1996)		Yang and Liu (2004)	Qian et al (2008)
T_1 (°K)[b]	6000	6000		6000	6000
T_2 (°K)	5918 (5)[a]	5967 (10)		5961 (7)	5953 (7)
q (M_2/M_1)[b]	0.381 (2)	0.381 (4)		0.381 (2)	0.376 (2)
A[b]	0.5	0.5		0.5	0.5
g[b]	0.32	0.32		0.32	0.32
$\Omega_1 = \Omega_2$	2.578 (2)	2.598 (9)		2.582 (7)	2.591 (4)
i°	83.06 (9)	82.43 (13)		83.87 (22)	84.43 (23)
$A_{Sp} = T_S/T_{primary}$	0.70	0.71	0.82	0.79	0.85
Θ_{Sp} (spot co-latitude)	90	90	90	90	115
ϕ_{Sp} (spot longitude)	180	180	25	180	180
r_{Sp} (angular radius)	15	15	12	10	16
$A_{Ss} = T_S/T_{secondary}$	-	-		0.81	1.1
Θ_{Ss} (spot co-latitude)	-	-		103	90
ϕ_{Ss} (spot longitude)	-	-		253	130
r_{Ss} (angular radius)	-	-		16	14
r_1(back)	0.5133	0.5090		0.5119	0.5067
r_1(side)	0.4822	0.4789		0.4811	0.4775
r_1(pole)	0.4485	0.4460		0.4477	0.4450
r_1(point)	0.5977	0.5977		0.5977	0.5989
r_2(back)	0.3481	0.3426		0.3463	0.3374
r_2(side)	0.3055	0.3023		0.3045	0.2989
r_2(pole)	0.2913	0.2887		0.2905	0.2857
r_2(point)	0.4023	0.4023		0.4023	0.4011
$\chi 2$ (B)[c]	0.015564	0.008312		0.014745	-
$\chi 2$ (V)	0.018513	0.010790		0.015369	0.008779
$\chi 2$ (I_c)	0.045351	-		-	-

a: Error estimates in parentheses correspond to least significant figure(s) for each value
b: Fixed elements during DC
c: $\chi 2$ (B, V or I_c) from PHOEBE (Prša and Zwitter 2005)

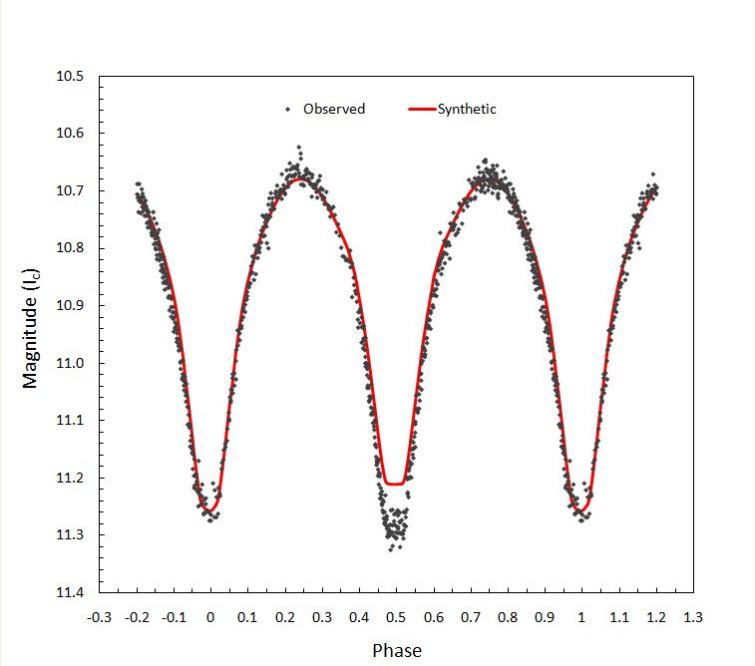

Figure 3.
Unspotted A-subtype Roche model fit of I_C bandpass light curve for RT LMi (2008). The synthesized curve significantly underestimates the secondary minimum at Min II without the addition of a cool spot on the primary star.

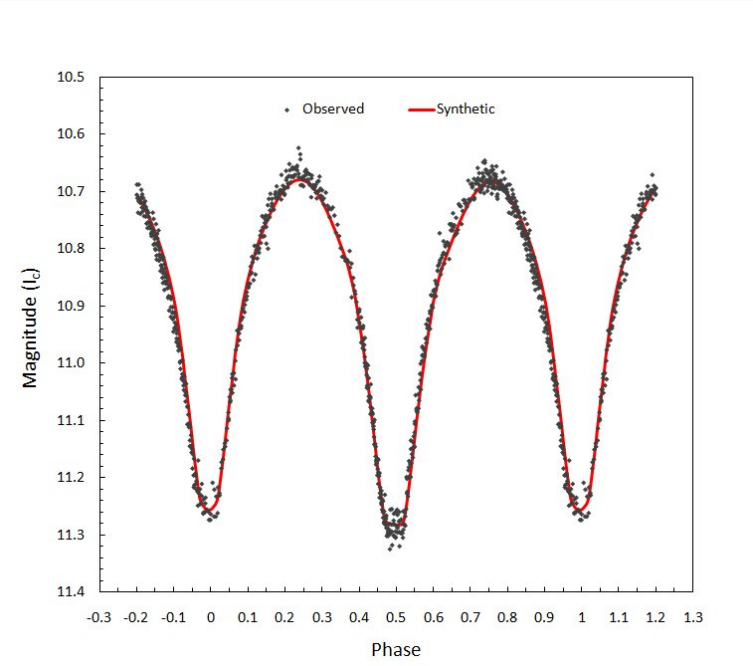

Figure 4.
A-subtype (T_1>T_2) Roche model fit of I_C bandpass light curve (2008) for RT LMi which positions a cool spot on the primary star facing the observer during Min II.

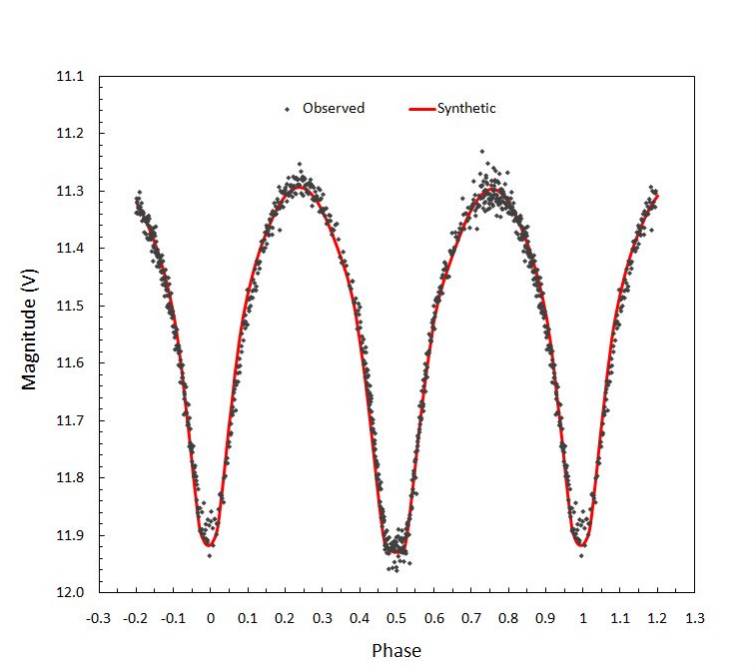

Figure 5.
A-subtype (T_1>T_2) Roche model fit of V bandpass light curve for RT LMi (2008) with cool spot positioned on the primary star facing the observer during Min II.

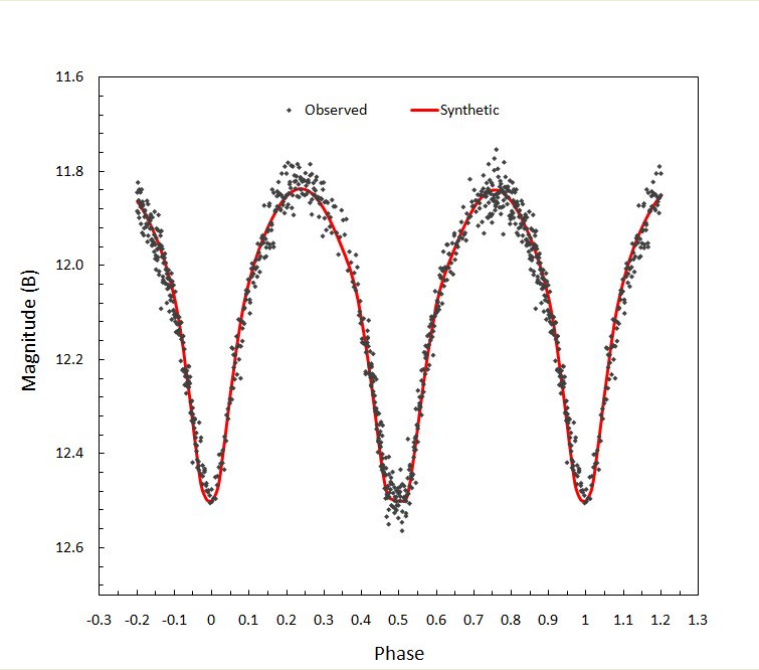

Figure 6.
A-subtype (T_1>T_2) Roche model fit of B bandpass light curve for RT LMi (2008) with cool spot positioned on the primary star facing the observer during Min II.

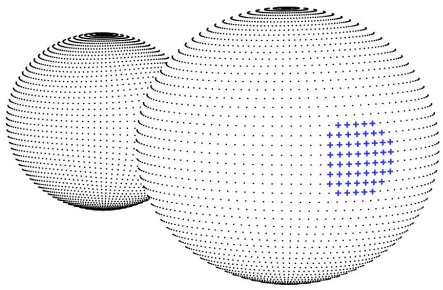

Figure 7.
A-subtype Roche model 3-D rendering of RT LMi showing position of cool spot on primary star.

T_2 (5918-5967 °K), i (82.43-84.43°), and $\Omega_{1,2}$ (2.578-2.598). The most provocative outcome from this study indicated that an A-subtype model requires the positioning of a cool spot on each primary star in generally the same location. This suggested the possibility of a persistent starspot feature which faces the viewer during Min II, yet RT LMi is the least active source of x-rays seen amongst fifty-seven W UMa type contact systems studied (Stepień et al 2001) using data from the ROSAT all-sky survey. This is contrary to what would appear to be the constant presence of a surface feature known to produce x-rays in other star systems. Furthermore, a second starspot was necessary to achieve an acceptable A-subtype solution in three out of four epochs. The introduction of another starspot increases the degrees of freedom in the model and further confounds the ability to arrive at a unique light curve solution. Perhaps another modeling strategy which makes fewer assumptions is in order for this binary system. Could a W-subtype arrangement (T_2>T_1) uniformly simplify the Roche model solution for this system?

3.4.2 W-Subtype

There is certainly precedence in the literature for other W UMa binary systems which seemingly vacillate between A- and W-subtypes. These include AH Cnc (Sandquist and Shetrone 2003; Qian et al 2006), AM Leo (Binnendijk 1969; Hoffmann and Hopp 1982), and TZ Boo (Hoffmann 1978, 1980; Awadalla 1989).

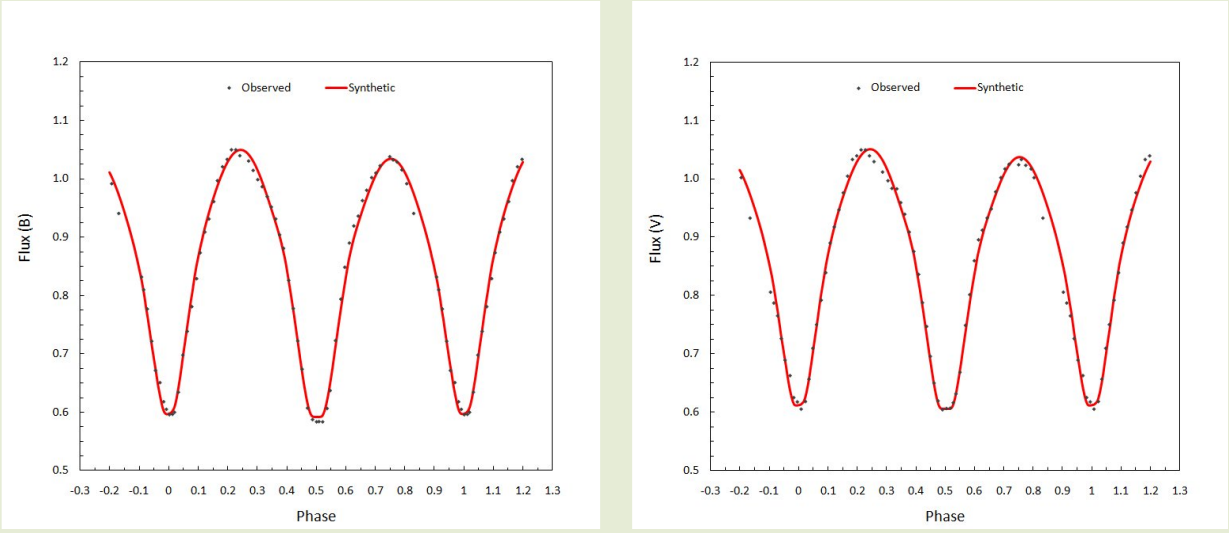

Figure 8.
A-subtype (T_1>T_2) Roche model fit of the rephased B (left) and V (right) light curves collected in 1982 (Niarchos et al 1994). Each newly synthesized fit for RT LMi involved the positioning of two cool spots on the primary star.

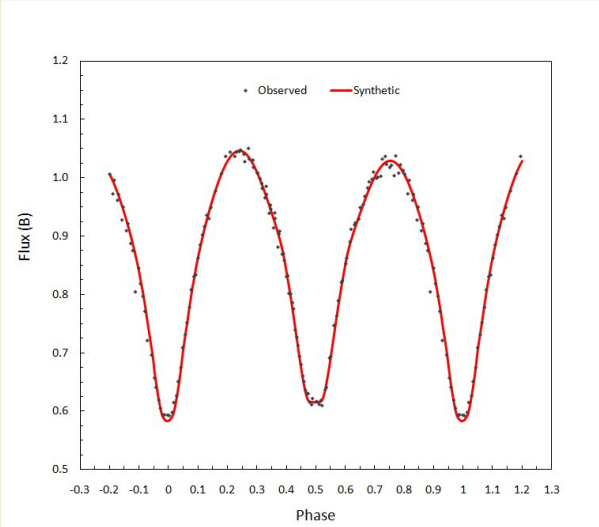

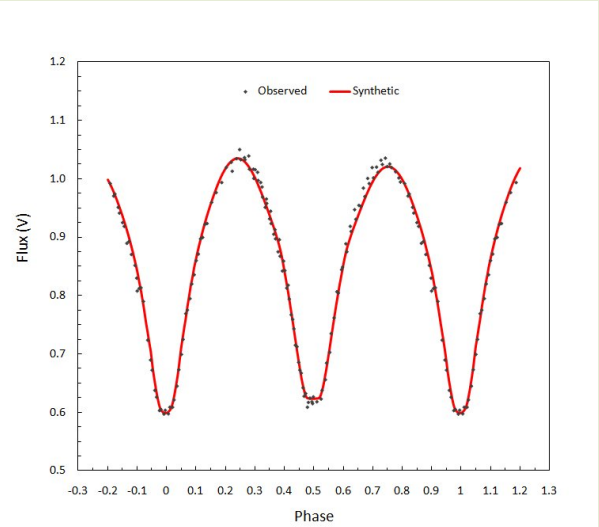

Figure 9.
A-subtype (T_1>T_2) Roche model fit of B (left) and V (right) light curves collected in 2003 (Yang and Liu 2004). Each newly synthesized fit for RT LMi involved the positioning of a cool spot on both the primary and secondary star.

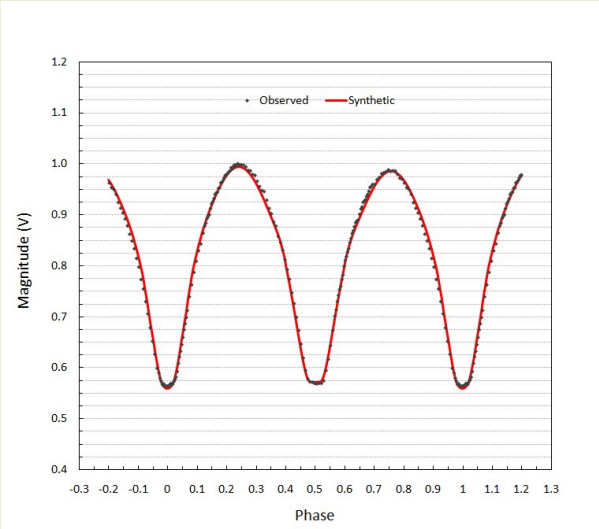

Figure 10.
A-subtype (T_1>T_2) Roche model fit of V passband light curve collected in 2001 (Qian et al 2008). This newly synthesized fit for RT LMi involved the positioning of a single cool spot on the primary and a hot spot on the secondary star.

With the exception of the 1982 light curve (Niarchos et al 1994) in which Min I and Min II may be inadvertently reversed as previously discussed, all other RT LMi light curves including the new one reported herein have shapes consistent with an A-subtype configuration. Yet, the 2001 (Qian et al 2008) and 2005 (Zola et al 2010) light curves were best fit using a higher temperature for the less-massive star thereby indicating W-subtype variation. Phased light curve data from the present study and those published by Niarchos et al (1994), Yang and Liu (2004), and Qian et al (2008) were subjected to Roche modeling as before, but this time T_2 was initially set at 6200 °K. Again for consistency, values for T_1 (6000 °K) and the mass ratio (0.381) were initially held constant while iteratively adjusting the effective temperature of the secondary (T_2), inclination (i), and common envelope surface potential ($\Omega_{1,2}$) until an acceptable fit of the model was obtained such that T_2>T_1. A comparison of light curve parameters and geometric elements obtained from Roche modeling is summarized in Table 5. Light curve fits from the present study are reproduced in Figs. 11 (I_c mag), 12 (V mag), and 13 (B mag); a geometric model for RT LMi with a cool

spot on the primary is shown in Fig. 14. The corresponding new fits to the previously published light curves are shown in Fig. 15 (Niarchos et al 1994), Fig. 16 (Yang and Liu 2004) and Fig. 17 (Qian et al 2008). Raw light curve data from Zola et al (2010) were not available and therefore a graphical representation could not be reproduced herein, however, selected geometrical and physical elements from their W-subtype fit are included in Table 5 for comparison. W-subtype solutions for all five tabulated epochs share similar orbital inclination (82.6-84.5°) and $\Omega_{1,2}$ (2.554-2.578) values. Except for Zola et al (2010) who adopted an effective temperature (6200 °K) more in line with an F7V spectral type (Jager and Nieuwenhuijzen 1987), all the others were modeled with T_1 fixed at 6000 °K (GoV). Accordingly, the best fit solutions for T_2 only varied from 6090 to 6139 °K. Importantly, no more than one starspot was required to model each light curve and with the exception of the 1982 light curves (Niarchos et al 1994) the χ^2 statistic for each of the other epochs indicated a better overall fit to the Roche model. Qian et al (2008) appropriately challenge the uniqueness of Binnendijk's classification (A- or W-subtype) of W UMa systems based on light curve shape alone. Their data, like those from Yang and Liu (2004), Zola et al (2010) and the present study exhibits behavior (Min I = transit of primary by secondary) consistent with A-type variation, yet the best fit solutions to the Roche model suggest a higher temperature (~100°K) for the less-massive secondary companion, an attribute normally associated with a W-subtype system. Furthermore, as pointed out by Zola et al (2010), the absence of the O'Connell effect or said differently light curve symmetry during quadrature does not necessarily eliminate the possibility of spot(s) which might influence light curve minima. This is dramatically apparent in the present study where a much deeper Min II appears in the 2008 light curves but can be modeled by invoking a cool spot on the surface of the primary which faces the observer during Min II (Figs. 7 and 14). The W-subtype solution for RT LMi therefore offers the advantage of simplicity (fewer starspots) across all light curves extant, as well as an overall improved goodness of fit (χ^2) to the Roche model.

Table 5. A Comparison of Selected Geometrical and Physical Elements for RT LMi Obtained Following Roche Model Light Curve Fitting as a W-subtype W UMa Binary System

Parameter	Present Study	Niarchos et al (1996)	Yang and Liu (2004)	Qian et al (2008)	Zola et al (2010)
T_1 (°K)[b]	6000	6000	6000	6000	6200
T_2 (°K)	6090 (2)[a]	6139 (6)	6077 (9)	6100 (7)	6350 (58)
q (M_2/M_1)[b]	0.381 (1)	0.381 (1)	0.382 (2)	0.381	0.382
A[b]	0.5	0.5	0.5	0.5	0.5
g[b]	0.32	0.32	0.32	0.32	0.32
$\Omega_1 = \Omega_2$	2.578 (2)	2.567 (6)	2.554 (5)	2.566 (3)	2.575 (24)
i°	84.50 (7)	83.21 (36)	82.62 (9)	84.28 (26)	83.2 (6)
$A_{Sp} = T_S/T_{primary}$	0.80	1.1	0.85	0.80	-
Θ_{Sp} (spot co-latitude)	90	90	90	90	-
ϕ_{Sp} (spot longitude)	172	350	35	90	-
r_{Sp} (angular radius)	10	12	15	10	-
r_1(back)	0.5131	0.5170	0.5146	0.5171	-
r_1(side)	0.4821	0.4851	0.4832	0.4851	0.4874
r_1(pole)	0.4484	0.4506	0.4492	0.4506	-
r_1(point)	0.5977	0.5977	0.5977	0.5977	-
r_2(back)	0.3479	0.3530	0.3498	0.3531	-
r_2(side)	0.3054	0.3082	0.3064	0.3083	0.3039
r_2(pole)	0.2912	0.2936	0.2921	0.2936	-
r_2(point)	0.4023	0.4023	0.4023	0.4023	-
χ^2 (B)[c]	0.014986	0.009520	0.014505	-	-
χ^2 (V)	0.015987	0.011153	0.016706	0.003815	
χ^2 (I_c)	0.040120	-	-	-	-

a: Error estimates in parentheses correspond to least significant figure(s) for each value
b: Fixed elements during DC
c: χ^2 (B, V or I_c) from PHOEBE (Prša and Zwitter 2005)

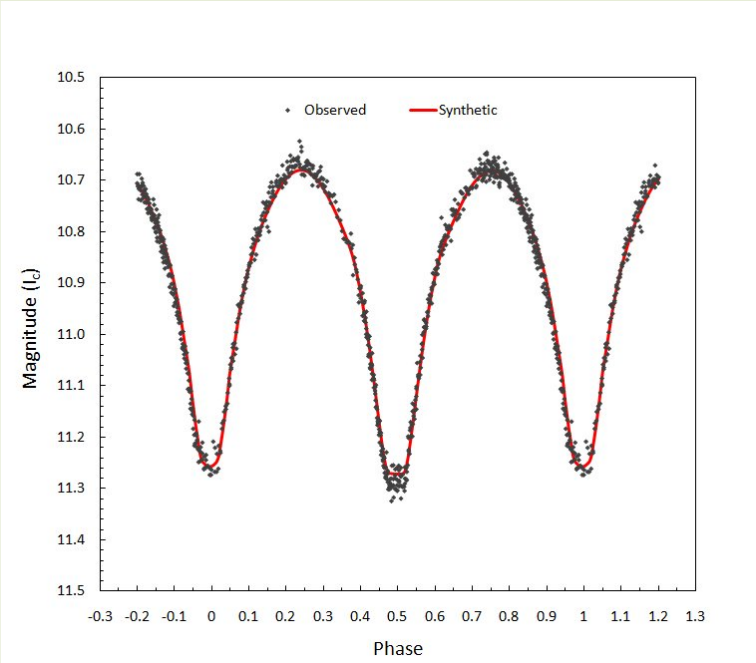

Figure 11.
W-subtype (T_2>T_1) Roche model fit of I_c bandpass light curve (2008) for RT LMi which positions a single cool spot on the primary star facing the observer during Min II.

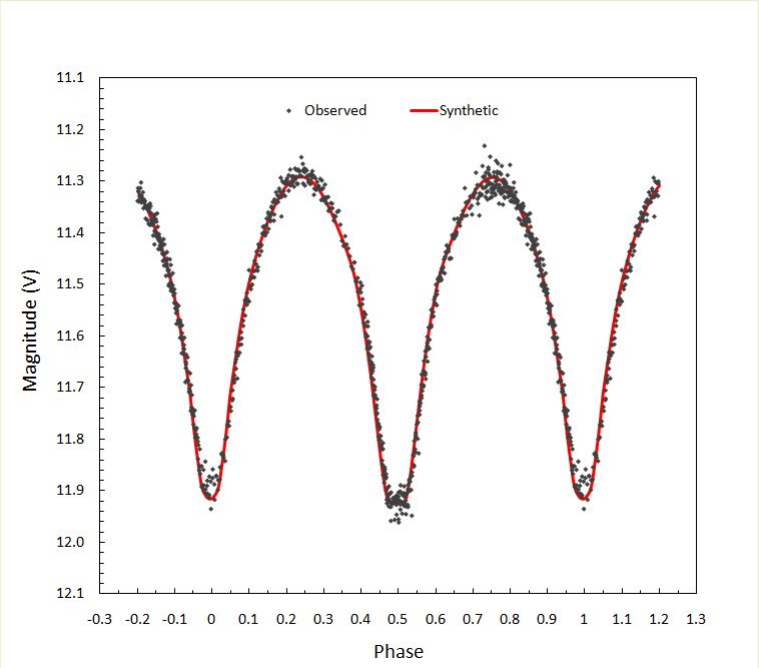

Figure 12.
W-subtype (T_2>T_1) Roche model fit of V bandpass light curve (2008) for RT LMi which positions a single cool spot on the primary star facing the observer during Min II.

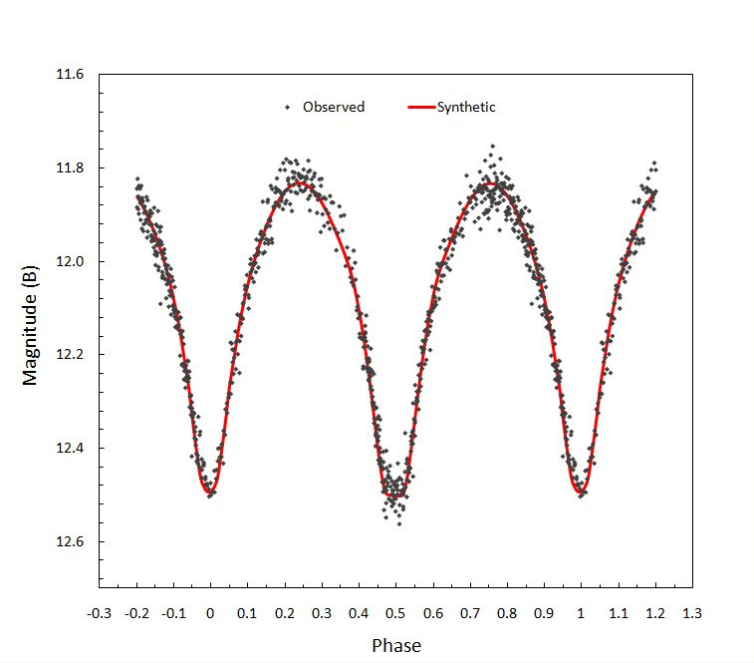

Figure 13.
W-subtype (T_2>T_1) Roche model fit of B bandpass light curve (2008) for RT LMi which positions a single cool spot on the primary star facing the observer during Min II.

4. Conclusions

New CCD photometric readings in B, V and I_c along with additional ToMs from the literature were used to update the linear ephemeris [Min. I (hel.) = 2,455,275.3476 + 0.37491747 E] for RT LMi. The O-C diagram exhibits sinusoidal-like short-term (~19.6 yr) changes often attributed to magnetic activity cycles. This is in contrast to much longer periods (47-64 yrs) proposed by two other research groups (Yang and Liu 2004; Qian et al 2008). With the exception of the 1982 light curve (Niarchos et al 1994) in which Min I and Min II may be inadvertently reversed, all other RT LMi light curves including the new one reported herein have shapes consistent with an A-subtype configuration. Yet, a direct comparison of A- and W-subtype solutions for the 2001 (Qian et al 2008), 2003 (Yang and Liu 2004) and the 2008 (present study) light curves shows that they were best fit using a higher temperature for the less-massive star thereby indicating a W-subtype variable system. In addition, Roche modeling according to the A-subtype convention where T_1>T_2 led to more complicated solutions in which a second starspot was required to achieve a satisfactory fit in three out of four epochs which were tested. By contrast, W-subtype solutions varied from having no spot (Zola et al 2010) to a single cool spot (Yang and Liu 2004; Qian et al 2008; present study) or a hot spot (Niarchos et al 1994) on the primary. By decreasing the number of starspots in the model there is a greater likelihood to arrive at a

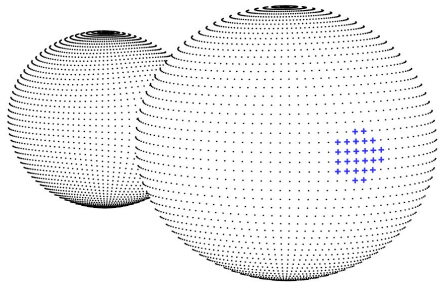

Figure 14.
3-Dimensional W-subtype (T_2>T_1) Roche model of RT LMi (2008) with cool spot positioned on the primary star (phase=0.6) surface which faces the viewer during Min II.

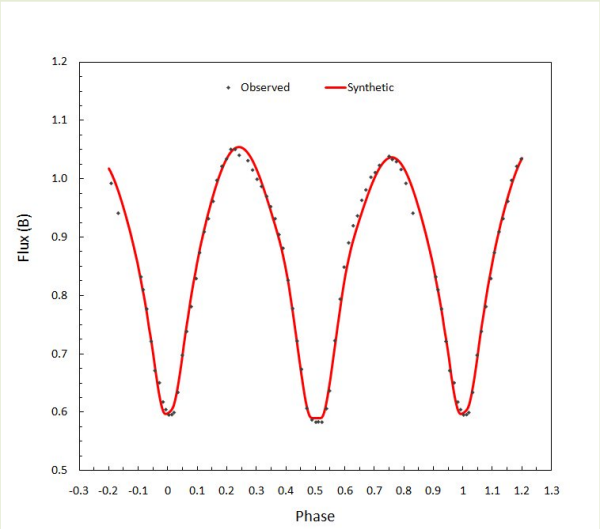

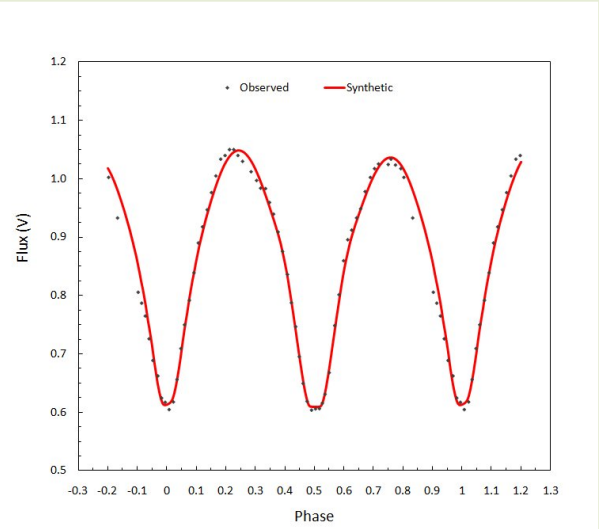

Figure 15.
W-subtype (T_2>T_1) Roche model fit of the rephased B (left) and V (right) light curves collected in 1982 (Niarchos et al 1994). Each newly synthesized fit for RT LMi involved the positioning of a single hot spot on the primary star.

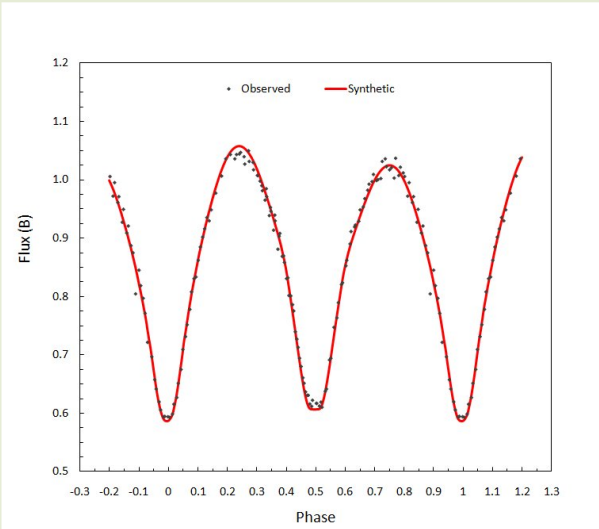

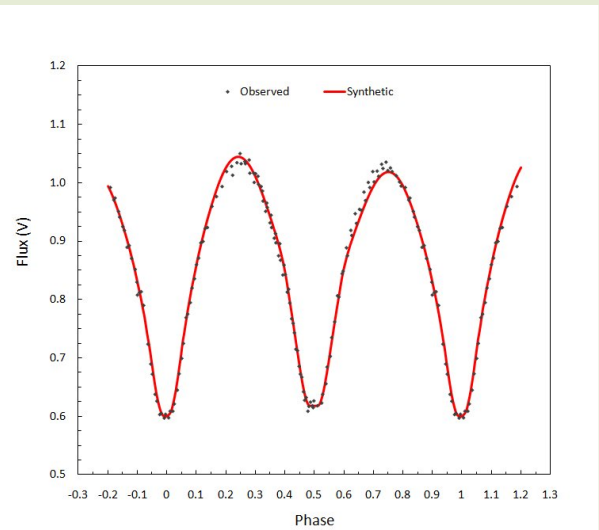

Figure 16.
W-subtype (T_2>T_1) Roche model fit of B (left) and V (right) light curves collected in 2003 (Yang and Liu 2004). Each newly synthesized fit for RT LMi involved the positioning of a single cool spot on the primary star.

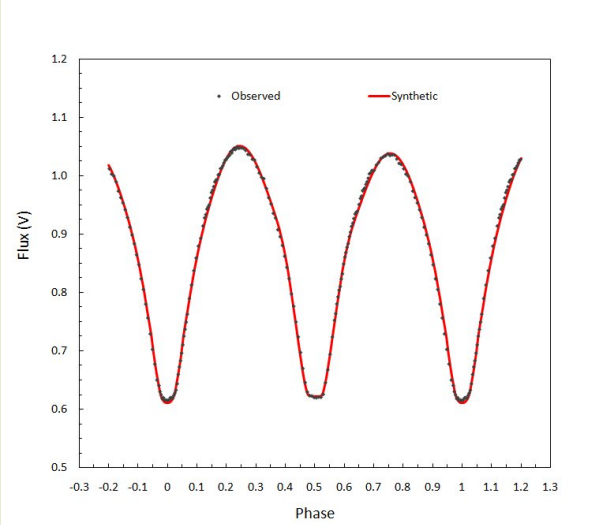

Figure 17.
W-subtype (T_1>T_2) Roche model fit of V passband light curve collected in 2001 (Qian et al 2008). This newly synthesized fit for RT LMi involved the positioning of a single cool spot on the primary star.

unique light curve solution. Overall, results from the present study provide a strong case for a unified W-subtype Roche model solution to all published light curves. The primary minimum for RT LMi results from the transit of a smaller but slightly hotter secondary while the flat-bottomed secondary minimum indicates that the cooler primary constituent completely occults its smaller cohort.

5. Acknowledgements

This research has made use of the SIMBAD database, operated at Centre de Données astronomiques de Strasbourg, France. Time-of-minima data from the B.R.N.O., IBVS, AASVO, and VSOLJ websites proved invaluable to the assessment of period changes experienced by this W UMa variable. The diligence and dedication shown by all associated with these organizations worldwide is very much appreciated. In addition, the SAO/NASA Astrophysics Data_System (http://adsabs.harvard.edu/abstract_service.html) was used to conduct literature searches in support of this study.

6. References

Agerer, F. 1996, IBVS, 4384.
Agerer, F. and Hübscher, J. 1997, IBVS, 4472.
Agerer, F. and Hübscher, J. 2002, IBVS, 5296.
Agerer, F. and Hübscher, J. 2003, IBVS, 5484.
Alton, K. 2009, JAAVSO, 37, 148.
Applegate, J.H. 1992, Astrophys. J., 385, 621.
Awadalla, N.S. and Hanna, M.A. 2005, J. Korean Astron. Society, 38, 43.
Awadalla, N.S. 1989, Astroph. and Space. Sci., 162, 211.
Berry, R., and Burnell, J. 2005, Handbook of Astronomical Image Processing,Willmann-Bell, Richmond.
Binnendijk, L. 1969, Astron. J., 74, 1031.
Binnendijk, L. 1970, Vistas Astron., 12, 217.
Borkovits, T., Elkhateeb, M. M., Csizmadia, Sz., Nuspl, J., Biró, I. B., Hegedüs, T., and Csorvási, R. 2005, Astron. and Astrophys., 441, 1087.
Bradstreet, D. H. and Steelman D. P. 2002, Bull. A.A.S., 34, 1224.
D'Angelo, C., van Kerkwijk, M.H. and Rucinski, S.M. 2006, Astron. J., 132, 650.
Diethelm, R. 2003, IBVS, 5438.
Diethelm, R. 2009, IBVS, 5894.
Diethelm, R. 2010, IBVS, 5945.
Dróżdż M. and Ogłoza, W. 2005, IBVS, 5623.
Dvorak, S.W. 2008, IBVS, 5814.
Flower, P.J. 1996, Astrophys. J., 469, 355.
Ghedini, S. 1981, Societa Astronomica Italiana, 52, 633.
Hamme, W. van 1993, Astron. J., 106, 2096.
Henden, A. A., and Kaitchuck, R. H. 1990, Astronomical Photometry: A Text and Handbook for the Advanced Amateur and Professional Astronomer, Willmann-Bell, Richmond.
Hoffmeister, C. 1949, Erg. Astron. Nachr., 288, 49.
Hoffmann, M. 1978, IBVS, 1487.
Hoffmann, M. 1983, IBVS, 2344.
Hoffmann, M. 1984, Veröff. Astron. Inst. Bonn, 96, 1.
Hoffmann, M. and Hopp, U. 1982, Astroph. and Space. Sci., 83, 391.
Hoffmann, M. and Meinunger, L. 1983, IBVS, 2343.
Hübscher, J. 2005, IBVS, 5643.
Hübscher, J. 2007, IBVS, 5802.
Hübscher, J., Lehmann, P.B., Monninger, G., Steinbach, H-M.W.F. 2010, IBVS, 5918.
Hübscher, J., and Monninger, G. 2011, IBVS, 5959.
Hübscher, J., Paschke, A. and Walter, F. 2005, IBVS, 5657.
Hübscher, J., Paschke, A. and Walter, F. 2006, IBVS, 5731.
Hübscher, J., Steinbach, H-M. and Walter, F. 2009, IBVS, 5874.
Jager, C. de and Nieuwenhuijzen, H. 1987, Astron. and Astrophys., 177, 217.
Kreiner, J.M. 2004, Acta Astronomica, 54, 207.
Kwee, K.K. and Woerden, H. van 1956, B.A.N., 12, 327.
Lucy, L. B. 1967, Z. Astrophys., 65, 89.
Minor Planet Observer 2010, MPO Software Suite, BDW Publishing, Colorado Springs (http://www.minorplanetobserver.com).
Nagai, K. 2003, VSOLJ, 40.

Nelson, R.H. 2004, IBVS, 5493.
Nelson, R.H. 2005a, IBVS, 5602.
Nelson, R.H. 2005b, "Eclipsing Binary O–C," URL: http://www.aavso.org/bob-nelsons-o-c-files.
Nelson, R.H. 2006, IBVS, 5672.
Nelson, R.H. 2007, "Minima©2002-2006: "Astronomy Software by Bob Nelson" URL: http://members.shaw.ca/bob.nelson/software1.htm
Nelson, R.H. 2009a, "WDwint56a: "Astronomy Software by Bob Nelson" URL: http://members.shaw.ca/bob.nelson/software1.htm
Nelson, R.H. 2009b, IBVS, 5875.
Niarchos, P.G., Hoffmann, M., and Duerbeck, H.W. 1994, Astron. and Astrophys., 103, 39.
Parimucha, Š., Dubovský, P., Baludanský, D. Pribulla, T., Hambálek, L., Vaňko, M. and Ogłoza, W. 2009, IBVS, 5898.
Parimucha, Š., Dubovský, P., Vaňko, M., Pribulla, T., Kudzej, I. and Barsa, R. 2011, IBVS, 5980.
Prša, A., and Zwitter, T. 2005, Astrophys J., 628, 1, 426.
Qian, S-B., Liu, L., Soonthornthum, B., Zhu, L-Y. and He, J-J. 2006, Astron. J., 131, 3028.
Qian, S-B., He, J-J. and Xiang, F-Y. 2008, Publ. Astron. Soc. Japan, 60, 77.
Ruciński, S. M. 1969, Acta Astron., 19, 245.
Ruciński, S. M., Lu, W. and Mochnacki, S.W. 2000, Astron. J., 120, 1133.
Samolyk, G. 2010, JAAVSO, 38, 85.
Sandquist, E.L. and Shetrone, M.D. 2003, Astrophys. J., 125, 2173.
Schwarzenberg-Czerny, A. 1996, Astrophys J., 460, L107.
Stepień, K., Schmitt, J.H.M.M. and Voges, W. 2001, Astron. and Astrophys., 370, 157.
Wilson, R.E. 1979, Astrophys. J., 234, 1054.
Wilson, R.E. and Devinney, E.J. 1971, Astrophys. J., 166, 605.
Yakut, K. and Eggleton, P.P. 2005, Astrophys. J., 629, 1055.
Yang, Y-L. and Liu, Q-Y. 2004, Chin. J. Astron. Astrophys., 4, 553.
Zola, S., Gazeas, K., Kreiner, J.M., Ogłoza, W., Siwak, M.,

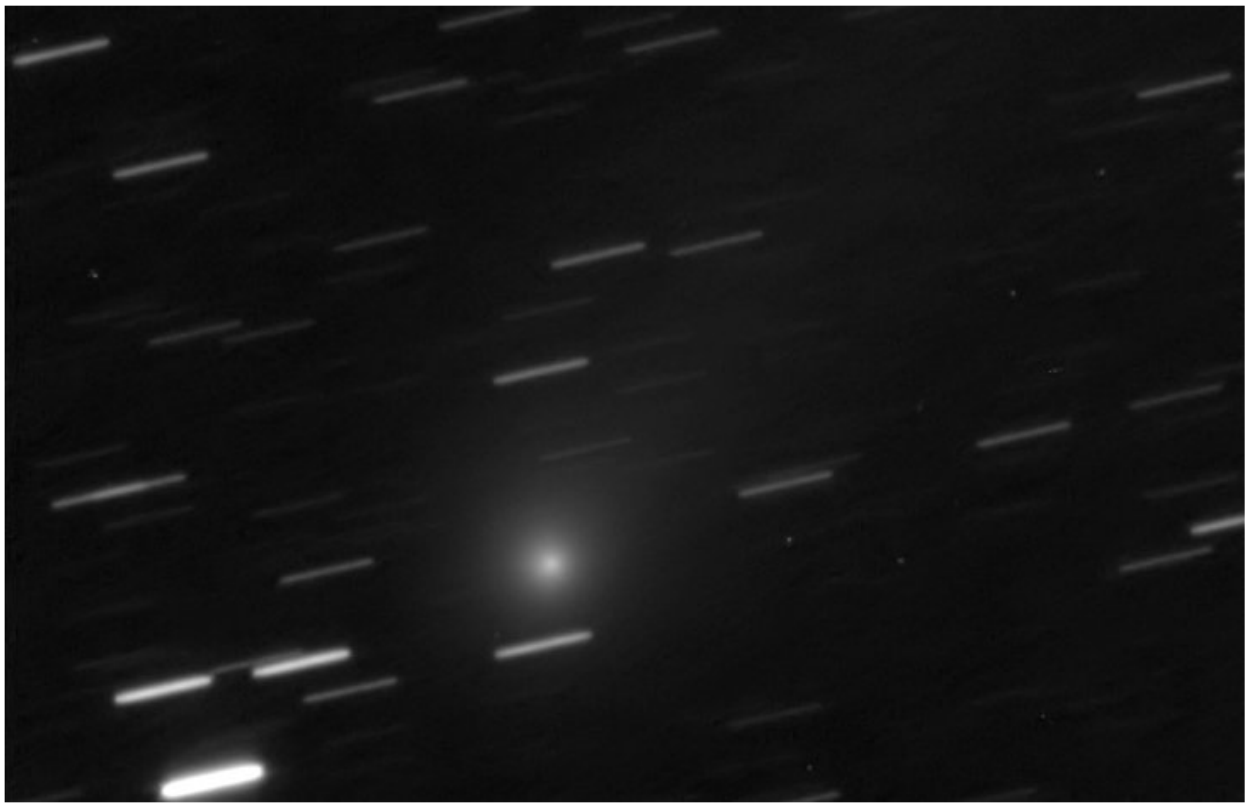

Comet C/2009 P1 Garradd

Composite of 50 stacked images (Vixen VC200L@ f/9 and ST-402ME-Ic filter) taken over a 25 min period as C/2009 P1 was making its way through Delphinus on 17Aug2011 @10:30 EDT.

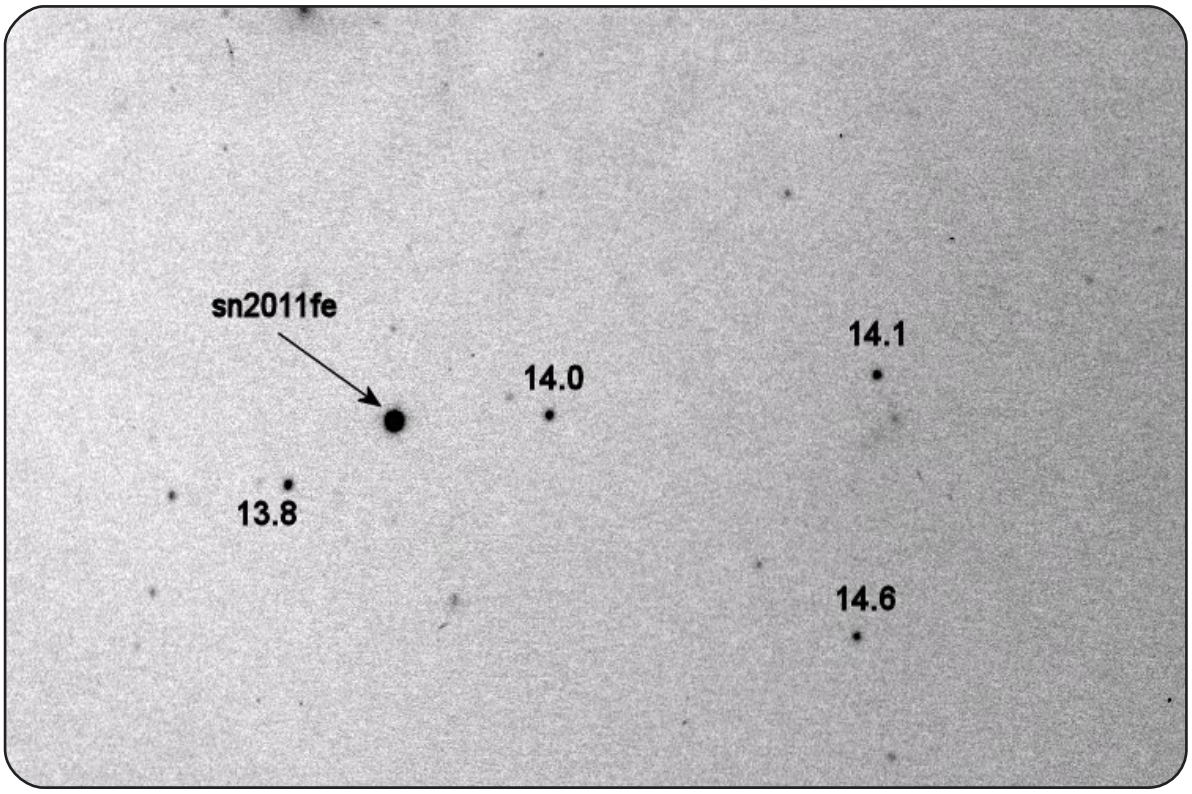

Supernovae: The Ultimate Variable Stars

Stacked (10 × 90 sec) image of SN2011fe in the Pinwheel Galaxy (M101) taken on 4Sept2011 (midtime=01:14:09 UTC) under hazy conditions. Equipment included a VC200L (f/9) coupled with an ST-402ME CCD camera (V band). The magnitude (V) of sn2011fe was estimated to be ~10.4 based upon AAVSO reference stars in same FOV. This should be an exciting object to monitor over the next few months.

In the Next Issue

KW Peg and BX Peg, Two Variables for the Price of One

Complete light curves for KW Peg (detached binary) and BX Peg (W UMa binary) were simultaneously collected in B, V and I_c passbands. Roche modeling provided potential solutions for these two binary systems located in the same FOV.

Photometry Basics Part III:

A lexicon for understanding variable star and light curve vernacular

Ovision Worm Gear Upgrade for a Losmandy G11

A recent upgrade of the OEM worm gear and mount tune-up has significantly improved the performance of this highly regarded GEM which has been a mainstay at UnderOak Observatory.